

2

4 **Evolution of the insecticide target *Rdl* in African**  
4 ***Anopheles* is driven by interspecific and**  
6 **interkaryotypic introgression**

6

8 Xavier Grau-Bové<sup>1\*</sup>, Sean Tomlinson<sup>1,2</sup>, Andrias O. O'Reilly<sup>3</sup>, Nicholas J. Harding<sup>4</sup>, Alistair Miles<sup>4,5</sup>,  
9 Dominic Kwiatkowski<sup>4,5</sup>, Martin J. Donnelly<sup>1,5</sup>, David Weetman<sup>1\*</sup>, The Anopheles gambiae 1000  
10 Genomes Consortium<sup>6</sup>

11 1. Department of Vector Biology, Liverpool School of Tropical Medicine, Liverpool, United  
12 Kingdom

13 2. Centre for Health Informatics, Computing and Statistics, Lancaster University, Lancaster,

14 3. School of Biological and Environmental Sciences, Liverpool John Moores University, Liverpool,  
15 UK

16 4. Big Data Institute, University of Oxford, Li Ka Shing Centre for Health Information and  
17 Discovery, United Kingdom

18 5. Wellcome Sanger Institute, Hinxton, United Kingdom

19 6. <https://www.malariagen.net/projects/ag1000g#people>

20 \* Corresponding authors: XGB ([xavier.graubove@gmail.com](mailto:xavier.graubove@gmail.com)), DW ([david.weetman@lstmed.ac.uk](mailto:david.weetman@lstmed.ac.uk))

## Abstract

22 The evolution of insecticide resistance mechanisms in natural populations of *Anopheles* malaria  
vectors is a major public health concern across Africa. Using genome sequence data, we study the  
24 evolution of resistance mutations in the *resistance to dieldrin locus (Rdl)*, a GABA receptor targeted  
by several insecticides, but most notably by the long-discontinued cyclodiene, dieldrin. The two  
26 *Rdl* resistance mutations (*296G* and *296S*) spread across West and Central African *Anopheles* via  
two independent hard selective sweeps that included likely compensatory nearby mutations, and  
28 were followed by a rare combination of introgression across species (from *A. gambiae* and *A.*  
*arabiensis* to *A. coluzzii*) and across non-concordant karyotypes of the 2La chromosomal inversion.  
30 *Rdl* resistance evolved in the 1950s as the first known adaptation to a large-scale insecticide-  
based intervention, but the evolutionary lessons from this system highlight contemporary and  
32 future dangers for management strategies designed to combat development of resistance in  
malaria vectors.

## 34 **Introduction**

36 The recurrent evolution of insecticide resistance in the highly-variable genomes of *Anopheles*  
38 mosquitoes (Neafsey et al. 2015; Miles et al. 2017; The *Anopheles gambiae* 1000 Genomes  
40 Consortium 2019) is a major impediment to the ongoing efforts to control malaria vector  
42 populations. Resistance to dieldrin was the first iteration of this cyclical challenge: this  
44 organochlorine insecticide was employed in a pioneering vector control programme in Nigeria in  
46 1954, but resistant *Anopheles* had already appeared after just 18 months (Elliott and Ramakrishna  
48 1956) due to a single dominant mutation (Davidson 1956; Davidson and Hamon 1962). Dieldrin  
use ceased in the 1970s due to its high persistence as an organic pollutant and unexpectedly wide  
toxicity, culminating in a ban by the 2001 Stockholm Convention on Persistent Organic  
Pollutants. However, resistance has remained strikingly persistent in natural *Anopheles*  
populations for more than 40 years (Du et al. 2005). The study of the genetic architecture of  
dieldrin resistance can thus provide key insights into the evolutionary ‘afterlife’ of resistance  
mechanisms to legacy insecticides. We address this issue by studying its emergence and  
dissemination in contemporary African populations of the *A. gambiae* species complex.

Dieldrin resistance in *Anopheles spp.* is caused by mutations in its target site, the  $\gamma$ -aminobutyric  
50 acid (GABA) receptor gene, a ligand-gated chloride channel also known as *resistance to dieldrin*  
*locus*—or *Rdl*—that is strongly conserved in a wide range of insects (ffrench-Constant, Rocheleau,  
52 et al. 1993; Thompson et al. 1993; Du et al. 2005). Two resistance mutations have been found in  
anophelines, both in codon 296: alanine-to-glycine (*A296G*) and alanine-to-serine (*A296S*).  
54 Resistant mutations in the homologous *Rdl* codon have also evolved in other insects, e.g. in  
*Drosophila spp.* (codon 302) (ffrench-Constant, Rocheleau, et al. 1993; Thompson et al. 1993; Du et  
56 al. 2005). Populations of *Anopheles gambiae* sensu stricto (henceforth, *A. gambiae*) and its sister  
species *A. coluzzii* possess both *296G* and *296S* alleles (Du et al. 2005; Lawniczak et al. 2010),  
58 whereas the *296S* allele is the only one reported in *A. arabiensis* and the more distantly-related  
malaria vectors *A. funestus* and *A. sinensis* (Du et al. 2005; Wondji et al. 2011; Yang et al. 2017).  
60 Normally, dieldrin inhibits the activity of *Rdl* receptors, causing persistent neuronal excitation  
and rapid death; but codon 296 mutations confer resistance by reducing its sensitivity to the  
62 insecticide (ffrench-Constant et al. 2000). However, in the absence of exposure, *Rdl* mutations  
appear to carry fitness costs, such as lower mosquito mating success (Platt et al. 2015) or  
64 impaired response to oviposition and predation-risk signals (Rowland 1991a; Rowland  
1991b) (although see (ffrench-Constant and Bass 2017)). Consequently, with seemingly limited  
66 current benefit via exposure to insecticides targeting *Rdl*, persistence of the mutations in

anophelines is puzzling.

68 We interrogate the *Anopheles gambiae* 1000 Genomes cohort (The *Anopheles gambiae* 1000 Genomes  
Consortium 2017; The *Anopheles gambiae* 1000 Genomes Consortium 2019) to ascertain how often  
70 dieldrin resistance mutations have evolved in the *A. gambiae*/*A. coluzzii* species pair, and the  
mechanisms by which these alleles spread across Africa and may persist. We identify two distinct  
72 *Rdl* resistance haplotypes in these species, defined by hard selective sweeps and the perfect  
linkage of the *296G* and *296S* alleles with putatively compensatory mutations. Furthermore, the  
74 resistance haplotypes are across genomes from different species (*A. gambiae*, *A. coluzzii* and *A.*  
*arabiensis*), and across chromosomes with differing karyotypes in the 2La inversion (the longest  
76 inversion in *Anopheles* genomes) (Coluzzi 2002) within which *Rdl* resides. Inter-species  
reproductive isolation and inversions such as 2La both result in reduced recombination rates  
78 (Sturtevant 1917; Andolfatto et al. 2001; Ayala and Coluzzi 2005; Kirkpatrick 2010), which would  
in principle hinder the spread of these adaptive alleles. Here, we provide evidence that *Rdl*  
80 resistance alleles, which our structural modelling shows have divergent effects on the channel  
pore, underwent a rare combination of interspecific and interkaryotypic introgression.

82 Overall, we show that two founding resistance mutations spread with remarkable ease across  
geographical distance, species, and recombination barriers. This evolutionary trajectory has  
84 parallels with later-emerging target site resistance mechanisms, such as knock-down resistance  
mutations in the *Vgsc* gene (Martinez-Torres et al. 1998; Davies et al. 2007; Clarkson et al. 2014;  
86 Clarkson et al. 2018). The persistence of dieldrin resistance also challenges the efficacy of current  
and newly developed insecticides that also target *Rdl* (Gant et al. 1998; Nakao and Banba 2015;  
88 Miglianico et al. 2018), as well as the efficacy of rotative insecticide management strategies  
(World Health Organization 2012). These results thus emphasise the influence of past  
90 interventions on current and future programmes of vector population control.

## 92 Results

### Distribution of *Rdl* resistance mutations across African populations

94 First, we investigated the genetic variation in *Rdl* across populations of the *Anopheles gambiae*  
 species complex, including *A. gambiae* and *A. coluzzii* from the *Anopheles gambiae* 1000 genomes  
 96 project (*Ag1000G* Phase 2,  $n = 1142$ ) (The *Anopheles gambiae* 1000 Genomes Consortium 2019), and  
 outgroups from four other species (*A. arabiensis*, *A. quadriannulatus*, *A. melas* and *A. merus*;  $n = 36$ )  
 98 (Fontaine et al. 2015). All genomes and their populations of origin are listed in Supplementary  
 Material SM1.

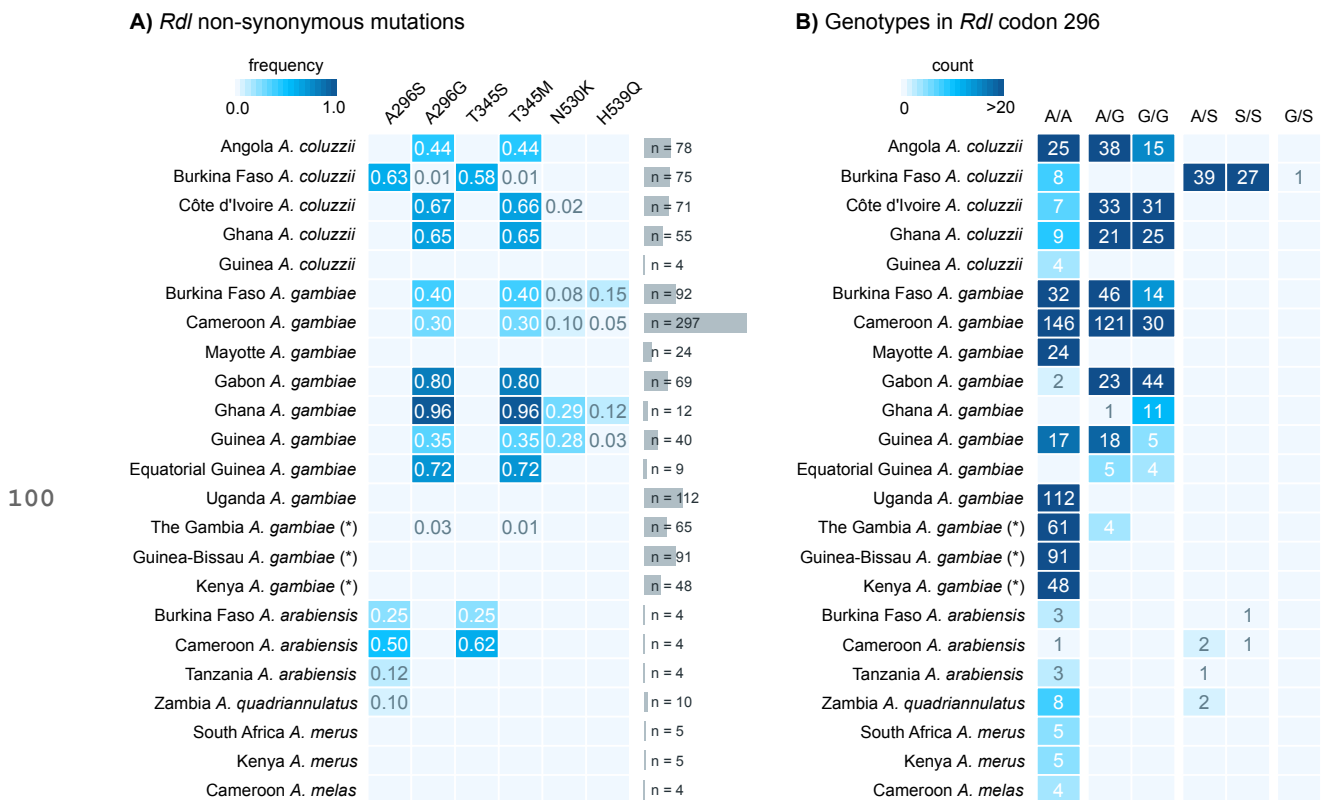


**Figure 1. *Rdl* mutations.** **A)** Frequency of non-synonymous mutations in *Rdl* across populations of *A. gambiae*, *A. coluzzii* (*Ag1000G* Phase 2) and *A. arabiensis*. Only variants with >5% frequency in at least on population are included. **B)** Distribution of genotypes for the two mutations in codon 296 (*A296S* and *A296G*). Note: *A. gambiae* populations denoted with an asterisk (The Gambia, Guinea-Bissau and Kenya) have high frequency of hybridisation and/or unclear species identification (see Methods).

We identified six non-synonymous mutations that are segregating in at least one population at  
 102  $\geq 5\%$  frequency (Figure 1A; complete list of variants in Supplementary Material SM2), including  
 the *296G* and *296S* resistance alleles. *296G* is present in West and Central African populations of  
 104 both *A. gambiae* and *A. coluzzii*, with frequencies ranging from 30% (Cameroon *A. gambiae*) to 96%  
 (Ghana *A. gambiae*). *296S* is present in *A. coluzzii* specimens from Burkina Faso (63%), as well as *A.*

106 *arabiensis* (Burkina Faso, Cameroon, Tanzania) and *A. quadriannulatus* (Zambia). Resistance alleles  
 occur as both homozygotes or heterozygotes in all species except *A. quadriannulatus*, which is  
 108 always heterozygous (Figure 1B).

We also identified two mutations in codon 345 with very similar frequencies to those of each  
 110 codon 296 mutation: *T345M* (C-to-T in the second codon position), co-occurring with *A296G*; and  
*T345S* (A-to-T in the first codon position), co-occurring with *A296S*. The high degree of linkage  
 112 disequilibrium between genotypes in codons 296 and 345 confirmed that they were co-occurring  
 in the same specimens (Figure 2; e.g., the *296G/345M* allele pair had a Huff and Rogers *r* and  
 114 Lewontin's  $D' = 1$ ), and was apparent in all individual populations where the alleles were present  
 (Supplementary Material SM3). Codons 296 and 345 are located in the 7th and 8th exons of *Rdl*,  
 116 separated by 3935 bp; and they map to the second and third transmembrane helices of the RDL  
 protein, respectively (Supplementary Material SM4).

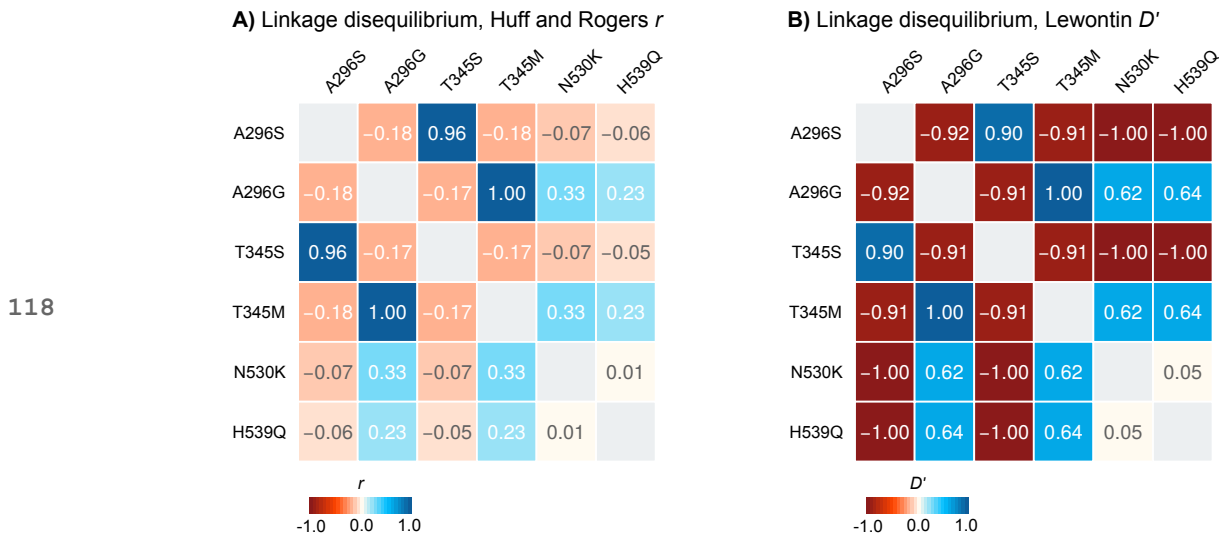
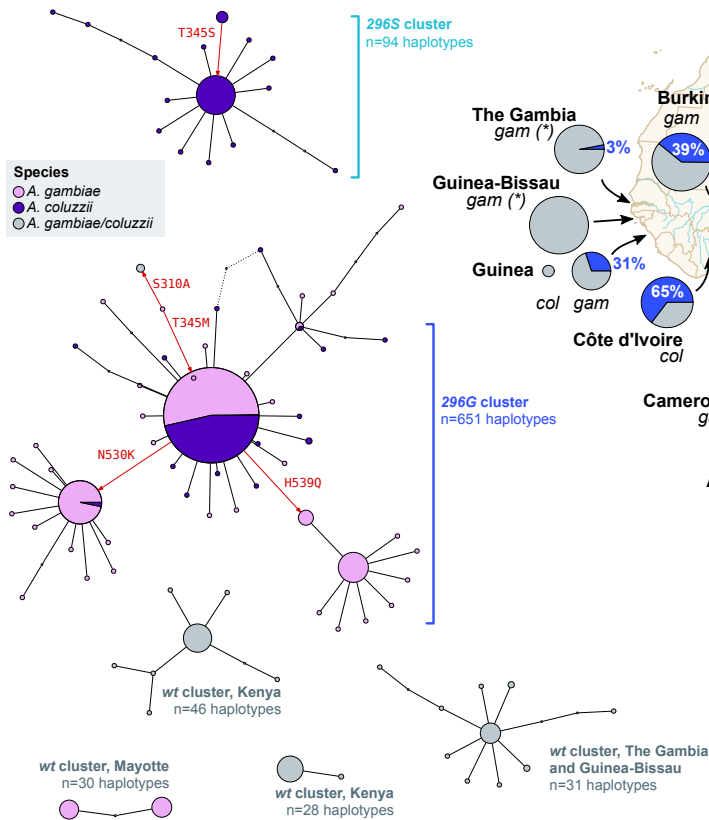


**Figure 2. Linkage disequilibrium.** Linkage disequilibrium between non-synonymous mutations in *Rdl*, calculated using Huff and Rogers' *r* (A) and Lewontin's  $D'$  (B).

## 120 ***Rdl* resistance mutations evolved on two unique haplotypes in *A. gambiae* and *A. coluzzii***

The high frequency of the *296S* and *296G* alleles in various populations of *A. gambiae* and *A. coluzzii*  
 122 (Figure 1), together with their co-occurrence with nearby mutations (Figure 2), were suggestive of  
 a selective sweep driven by positive selection on the resistance alleles. To clarify this possibility,  
 124 we inspected the similarity of haplotypes in *A. gambiae*, *A. coluzzii* and the four outgroup species ( $n$   
 = 2356 haplotypes) using a minimum spanning network based on 626 phased variants located  
 126 10,000 bp upstream and downstream of codon 296 (Figure 3).

**A) Minimum spanning network of haplotypes in *Rdl***



**B) Frequency of *Rdl* codon 296 haplotypes per population**

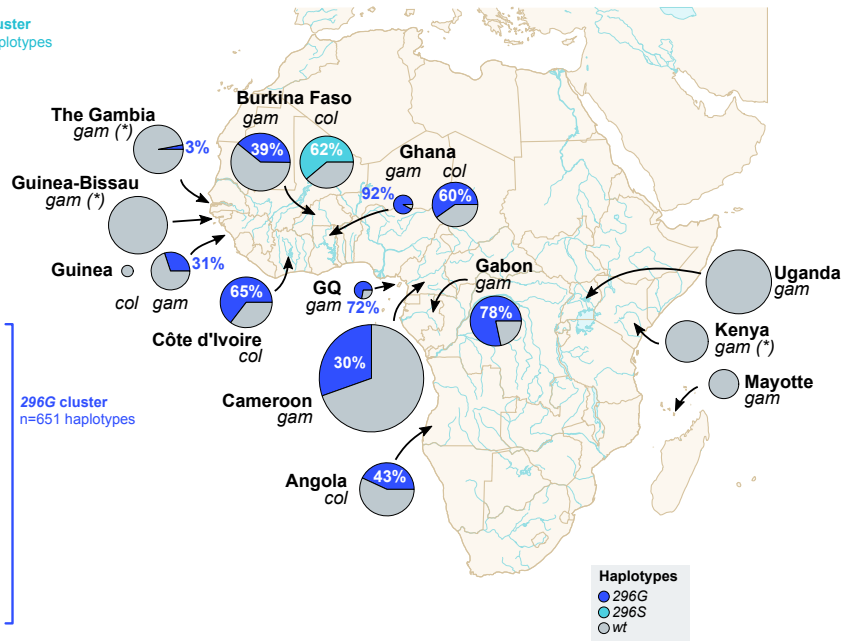


**Figure 3. *Rdl* haplotypes.** **A)** Minimum spanning network of haplotypes around *Rdl* codon 296 (626 phased variants located +/- 10,000 bp from the 2L:25429236 position). Only haplotype clusters with a frequency >1% in the cohort are represented (complete networks available as Supplementary Material SM6). Each node in the network is color-coded according to its species composition. Haplotype clusters carrying the resistance alleles 296G and 296S are highlighted in blue. Red arrows indicate the direction of non-synonymous mutations (relative to reference genome). **B)** Frequency of resistance haplotypes per population. Pie area reflects sample size, ranging from Guinea *A. coluzzii* ( $n = 8$ ) to Cameroon *A. gambiae* ( $n = 594$ ). Detailed frequencies with absolute counts in Supplementary Material SM14. Note: *gam*=*A. gambiae*, *col*=*A. coluzzii*; *gam* populations denoted with an asterisk have unclear species identification and/or high rates of hybridisation.

128 We identified two distinct groups of haplotypes associated with resistance mutations. First, the  
 296G cluster contained haplotypes sharing the 296G/345M alleles which were widely distributed  
 130 in Central and West Africa (11 populations of *A. coluzzii* and *A. gambiae*;  $n = 651$  haplotypes). The  
 296G group showed two sub-clusters associated with the downstream mutations N530K and  
 132 H539Q (red arrows in Figure 3A), which were present in a subset of mostly *A. gambiae* populations  
 (Guinea, Ghana, Burkina Faso and Cameroon; Figure 1A); with just a few *A. coluzzii* from Côte  
 134 d'Ivoire in the N530K cluster. Both N530K and H539Q are in partial linkage disequilibrium with  
 296G alleles (Figure 2).

136 In contrast, the 296S cluster, defined by ubiquitous co-occurrence of the 296S/345S allele pair, was  
 restricted to *A. coluzzii* from Burkina Faso ( $n = 94$ ; Figure 3A, B), whereas the *A. arabiensis* and *A.*

138 *quadriannulatus* 296S haplotypes appeared as distantly related singletons (not visible on Figure 3,  
see Supplementary Material SM5 and SM6). We also found four smaller wild-type clusters (296A  
140 allele; henceforth *wt*) that are specific to other geographical locations (Kenya, Mayotte, and The  
Gambia/Guinea-Bissau). The remaining haplotypes are also *wt* and group in smaller clusters or  
142 singletons with frequencies <1% in the dataset ( $n = 1476$ , 62.6% of all examined haplotypes;  
Supplementary Material SM5 and SM6).

144 Both the 296G and 296S haplotype clusters are often found in high frequencies within their  
respective populations. For example, 296S was present in 62.3% of all Burkinabè *A. coluzzii*, and  
146 296G reached 91.7% in Ghanaian *A. gambiae* (Figure 3B).

The haplotype clustering analysis shows that all non-synonymous mutations (*T345M*, *T345S*,  
148 *N530K*, and *H539Q*) are associated with either the 296G or the 296S resistance haplotypes. The  
existence of seven non-synonymous mutations associated in haplotypes that have evolved over  
150 the last 70 years is remarkable: mosquito *Rdl* genes are highly conserved and have accumulated  
very few amino-acid mutations since anophelines diverged from culicines (for instance, *A.*  
152 *gambiae Rdl* retains a 97.6% amino-acidic identity with its *Aedes aegypti* ortholog and  $d_N/d_S = 0.052$ ,  
indicating predominant purifying selection; Supplementary Material SM4). Here, we observe that  
154 the resistant haplotypes accumulate an excess of non-synonymous mutations compared to the *wt*,  
with non-synonymous to synonymous genetic diversity ratios ( $\pi_N/\pi_S$ ) being ~18x higher in the  
156 296G cluster ( $\pi_N/\pi_S = 2.428 \pm 0.009$  standard error) than in *wt* haplotypes ( $\pi_N/\pi_S = 0.135 \pm$   
0.001); and ~4x higher in 296S ( $\pi_N/\pi_S = 0.485 \pm 0.018$ ).

### 158 **The 296S and 296G alleles are associated with hard selective sweeps**

Next, we investigated the signals of positive selection linked to the 296S and 296G resistance  
160 haplotypes. First, we found that haplotypes carrying 296G and 296S alleles had longer regions of  
high extended haplotype homozygosity (*EHH*) than the *wt* (Figure 4A), as expected under a  
162 scenario of selective sweeps linked to these resistant variants. A closer examination revealed that  
*EHH* decays slower at the 3' region of *Rdl* (Figure 4A): in both clusters, *EHH* is above 0.95 (i.e. 95%  
164 of identical haplotypes) in the region downstream of codon 296 (exons 7 and 8), but decays more  
rapidly towards the 5' of the gene (*EHH* < 0.20 in exon 6a/6b, *EHH* < 0.10 in exon 1). The core  
166 resistance haplotypes had lengths of 5,344 bp for 296G and 4,161 bp for 296S (defined at *EHH* >  
95%), which were one order of magnitude higher than *wt* haplotypes (460 bp), and covered all  
168 non-synonymous mutations linked to codon 296 alleles (*T345M*, *T345S*, *N530K*, and *H539Q*).

Next, to estimate the softness/hardness of the sweep, we calculated the profile of Garud's *H*



170 statistics (Garud et al. 2015) and haplotypic diversity along the 2L chromosome arm (Figure 4B-  
 D). Both *296G* and *296S* haplotype clusters showed signals of a hard selective sweep: (i) they had  
 172 markedly higher Garud's  $H_{12}$  (*296G*: 0.698  $\pm$  0.001 standard error; *296S*: 0.744  $\pm$  0.006) than *wt*  
 (0.003  $\pm$  0.0), which indicates an over-abundance of the most frequent haplotypes in the cohort  
 174 (Messer and Petrov 2013; Garud et al. 2015); (ii) lower  $H_2/H_1$  ratios (*296G*: 0.052  $\pm$  0.0; *296S*:  
 0.011  $\pm$  0.007) than *wt* (0.756  $\pm$  0.001), indicative of a hard sweep with decreased background  
 176 variation (Messer and Petrov 2013; Garud et al. 2015); and (iii) low haplotypic diversity (*296G*:  
 0.501  $\pm$  0.001; *296S*: 0.377  $\pm$  0.007) compared to the *wt* (0.998  $\pm$  0.000).

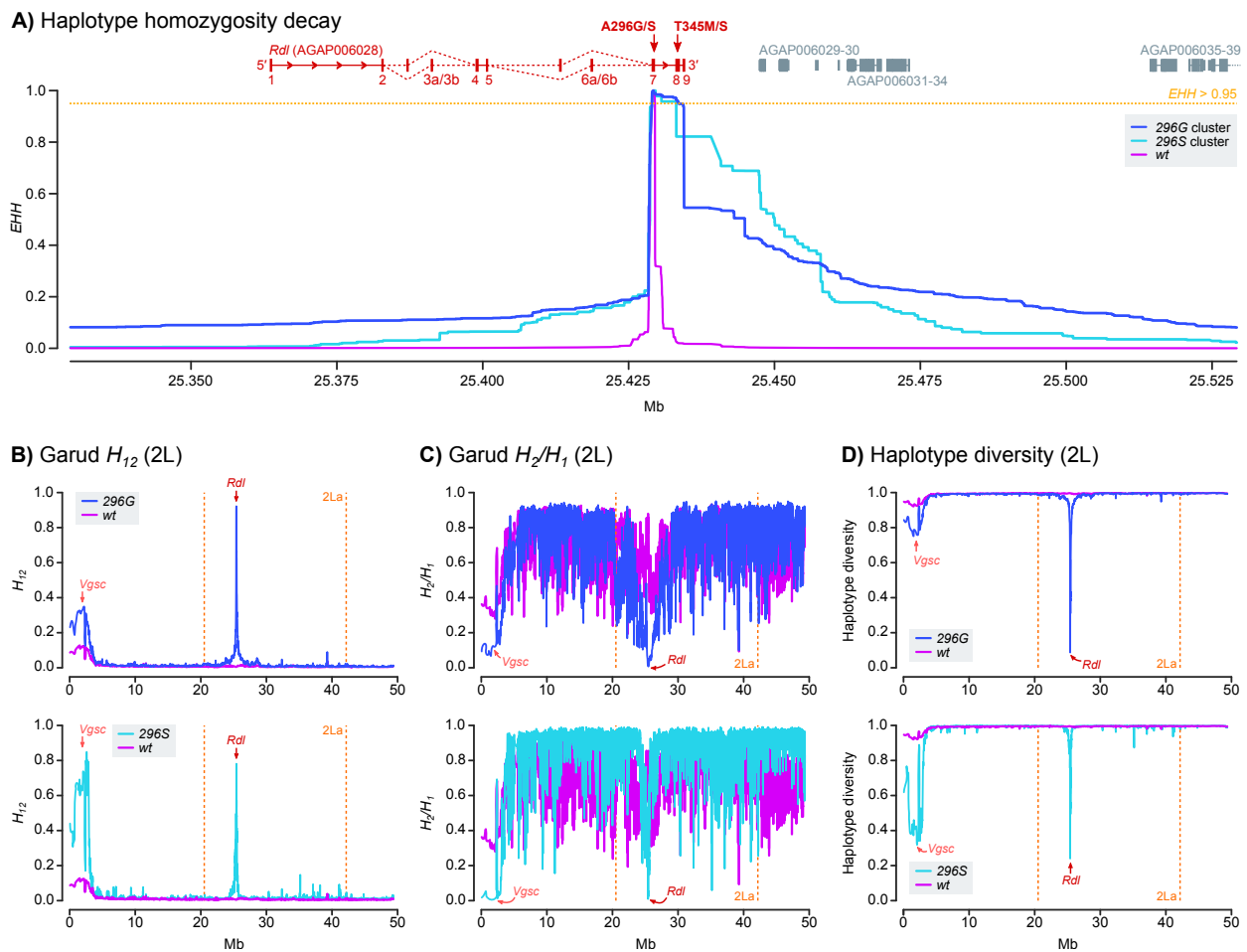


**Figure 4. Positive selection of haplotypes carrying resistance mutations.** **A)** Profile of  $EHH$  decay for each group of haplotypes (*296G*, *296S* and *wt*), built from 11,180 phased variants located  $\pm$  100,000 bp from codon 296 (2L:25429236 position). Coordinates of nearby genes are indicated above the  $EHH$  panel (in *Rdl*, exons are numbered and red arrows indicate the position of codons 296 and 345). **B-D)** Profiles of Garud  $H_{12}$ , Garud  $H_2/H_1$  and haplotypic diversity along chromosomal arm 2L, highlighting the region covered by the 2La inversion (orange vertical lines) and the location of *Rdl* (red arrow). Each statistic was calculated separately for haplotypes carrying the *296G*, *296S* and *wt* alleles, using sliding blocks of 500 variants with 20% overlap.

178 Unexpectedly, chromosomes containing *296G* and *296S* alleles also exhibited signals of positive  
 180 selection at a distant pericentromeric region of 2L (Figure 4B-D), typically associated with strong

selective sweeps around the *Vgsc* gene (Lynd et al. 2010; Clarkson et al. 2014; Clarkson et al.  
182 2018), which is the target site of pyrethroids and DDT (Davies et al. 2007). *Vgsc* selective sweeps  
are linked to two non-synonymous substitutions that confer resistance to these insecticides – the  
184 *L995F* and *L995S* knock-down resistance (*kdr*) mutations, commonly known as *L1014F* and *L1014S*  
after their codon coordinates in *Musca domestica* (Clarkson et al. 2018). Positive selection in *Vgsc*  
186 was particularly strong in chromosomes that also carried *296S* alleles ( $H_{12} = 0.917 \pm 0.004$   
standard error), followed by *296G* ( $H_{12} = 0.412 \pm 0.001$ ) and, to a lesser degree, *wt* ( $H_{12} = 0.147 \pm$   
188  $0.000$ ). However, neither of the *Vgsc kdr* alleles (*995F* and *995S*) are in linkage disequilibrium  
with *296G* or *296S* (Supplementary Material SM7, SM8). Rather, this apparent association is due to  
190 geographical overlap: *296G* and *296S* are present in West African populations that are near-fixed  
for *Vgsc* resistance alleles (>80% *995F* in 7 out of 10 populations; Supplementary Material SM8),  
192 but are mostly absent elsewhere.

Overall, *Rdl* resistance alleles are found on two unique sets of highly similar haplotypes (Figure 3),  
194 each of them specific to one allele (*296S* and *296G*), that underwent independent hard selective  
sweeps (Figure 4).

## 196 **Co-segregation of *Rdl* haplotypes and 2La inversions**

*Rdl* lies within the 2La chromosomal inversion, which is the longest in the *A. gambiae* genome  
198 (20.5-42.1 Mb) (Coluzzi 2002). The 2La inversion emerged in the last common ancestor of the *A.*  
*gambiae* species complex (Fontaine et al. 2015) and is currently polymorphic in *A. gambiae* and *A.*  
200 *coluzzii* (Stump et al. 2007), where it is linked to a range of important phenotypes including  
adaptation to human environments (Coluzzi et al. 1979), aridity (Cheng et al. 2012), insecticide  
202 resistance (Weetman et al. 2018), and susceptibility to *Plasmodium falciparum* (Riehle et al. 2017).  
Given that recombination is strongly reduced between chromosomes with discordant inversion  
204 karyotypes (Andolfatto et al. 2001; Ayala and Coluzzi 2005; Kirkpatrick 2010), any assessment of  
the evolution of genes within the 2La inversion, such as *Rdl*, needs to take into consideration  
206 whether haplotypes reside in inverted (2La) or non-inverted (2L<sup>+</sup>) backgrounds.

To address this issue, we estimated the 2La inversion karyotypes for the *Ag1000G* Phase 2  
208 samples using a principal component analysis of allele presence/absence in the inverted region  
(using genomes with known inversion karyotypes as a reference; Figure 5A and Supplementary  
210 Material SM1 and SM9). The first principal component clearly discriminated between each of the  
inversion genotypes (non-inverted 2L<sup>+</sup>/2L<sup>+</sup> homozygotes, inverted 2La/2La homozygotes, and  
212 2La/2L<sup>+</sup> heterozygotes). We used this information to compare the frequencies of 2La karyotypes

with *Rdl* codon 296 genotypes (Figure 5B), and the karyotype frequencies per population (Figure 5C). The pan-African 296G allele is present in all inversion karyotypes, but is more common in non-inverted backgrounds (73% of 296G/296G homozygotes have 2L<sup>+</sup>/2L<sup>+</sup> karyotypes; Figure 5B), in both *A. gambiae* and *A. coluzzii* populations (Figure 5C). On the other hand, 296S alleles from *A. arabiensis* and Burkinaabè *A. coluzzii* occur exclusively within the 2La inversion (100% of 296S/296S homozygotes are in 2La/2La karyotypes; Figure 5B).

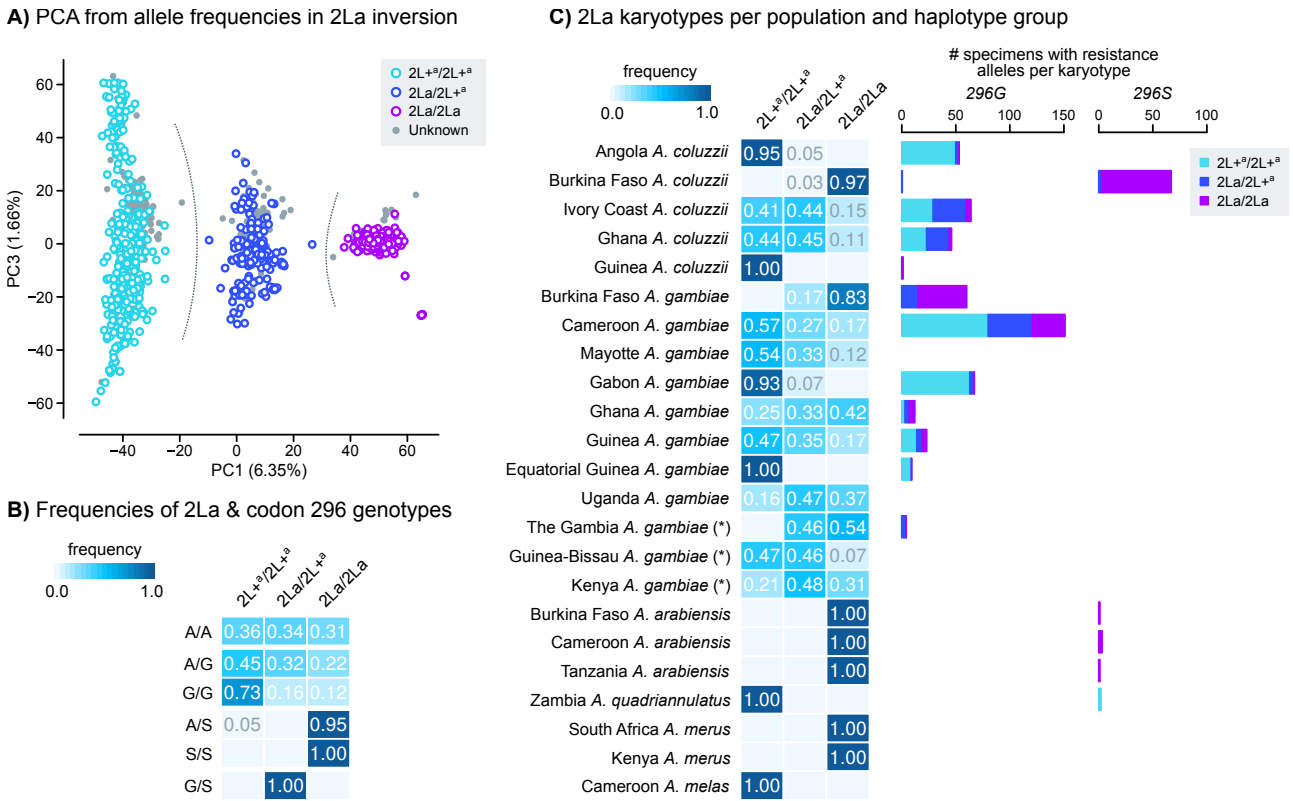


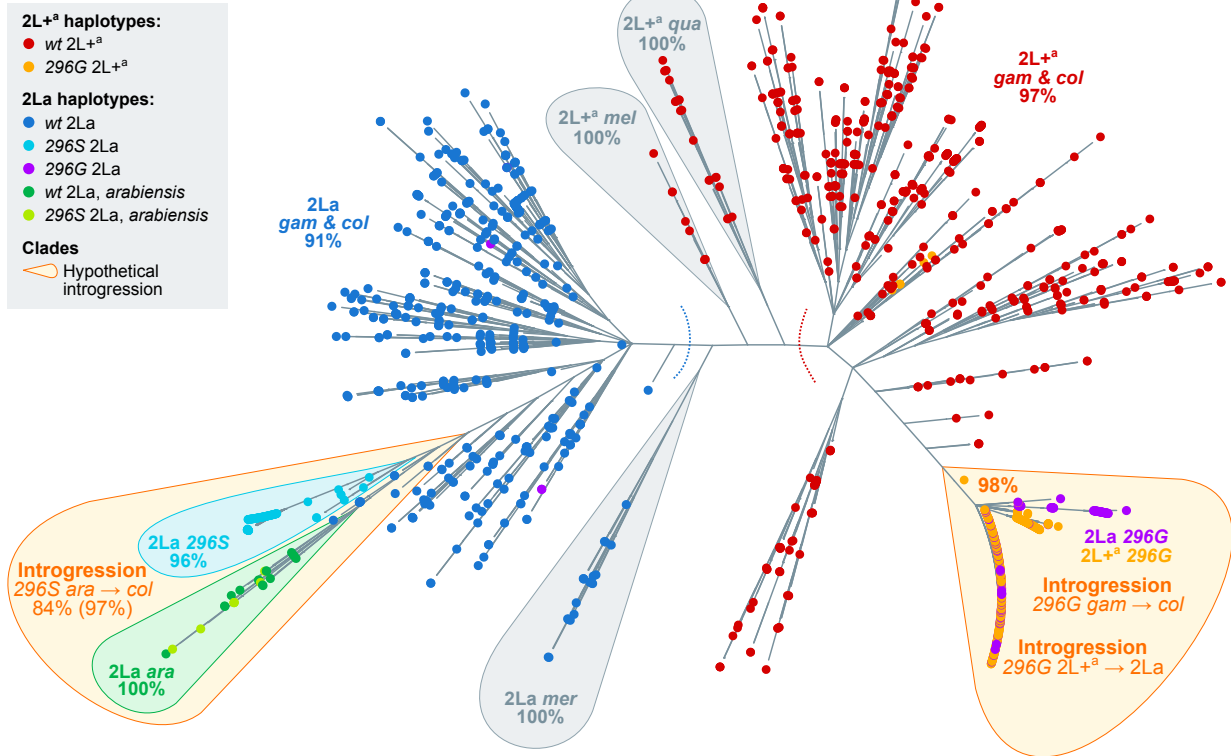
**Figure 5. Genotypes of the 2La inversion.** **A)** Principal component analysis of genotype frequencies of 10,000 random variants located within the 2La inversion (coordinates: 2L:20524058-42165532). Specimens from *Ag1000G* Phase 1 are color-coded by 2La karyotype (homozygotes and heterozygotes), and they are used as a reference to assign 2La genotypes to Phase 2 specimens (grey). Grey dotted lines highlight the separation of three clusters according to 2La karyotype. **B)** Frequency of 2La inversion and *Rdl* codon 296 genotypes. **C)** Frequency of 2La inversion karyotypes per population (heatmap, left), and number of specimens from each population carrying resistance alleles (296G and 296S), broken down by 2La karyotype (barplots, right). Note: *A. gambiae* populations denoted with an asterisk (The Gambia, Guinea-Bissau and Kenya) have high frequency of hybridisation and/or unclear species identification (see Methods).

## 220 Introgression of *Rdl* resistance haplotypes

In order to obtain a more complete picture of possible introgression events, we performed a phylogenetic analysis of haplotype alignments at four loci around *Rdl*: 5' and 3' regions of the gene, and two loci upstream and downstream of the gene body (Figure 6). These phylogenies highlight two events of interspecific introgression (explored below in grater detail): 296G between

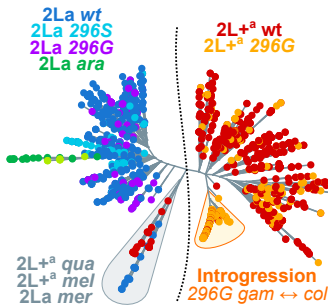
*A. gambiae* and *A. coluzzii* (as reflected by their identical swept haplotypes; Figure 3), and 296*S* between *A. coluzzii* and *A. arabiensis*. In addition, they also confirm the spread of 296*G* haplotypes across different 2La inversion types (interkaryotypic introgression; Figure 5). In the following paragraphs, we characterise these introgressions and attempt to identify the donors and acceptors of each event.

A) *Rdl* 3' region

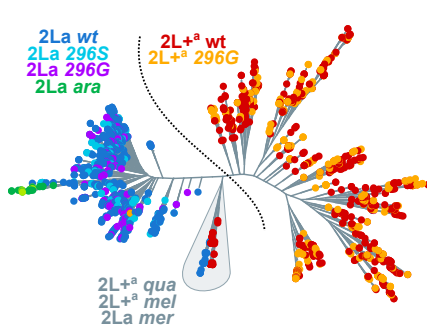


230

B) *Rdl* 5' region



C) 1 Mb upstream to *Rdl*



D) 1 Mb downstream to *Rdl*

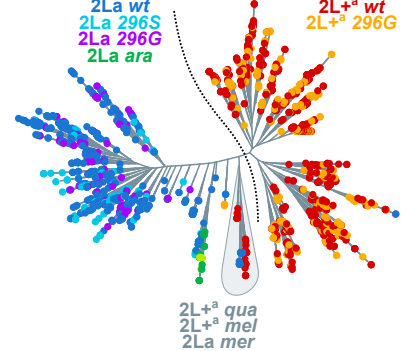


**Figure 6. Phylogenies of haplotypes around the *Rdl* locus.** A) Maximum-likelihood phylogenetic analysis of variants present at the 3' region of *Rdl* (20,000 kbp). Nodes are haplotypes and have been color-coded according to their *Rdl* genotype (296*S*, 296*G*, wt), 2La karyotype (2La, 2L<sup>+</sup>) and species. Orange bubbles highlight clades with hypothetical introgression events. Grey bubbles highlight outgroup clades. Statistical supports are shown on selected clades (UF bootstrap). B-D) Analogous phylogenies from the *Rdl* 5' region, upstream, and downstream regions within the 2La inversion (+/- 1 Mb of *Rdl*). Complete alignments and phylogenies in Supplementary Material SM10 and SM11. Species abbreviations: *col*=*coluzzii*, *gam*=*gambiae*, *ara*=*arabiensis*, *mer*=*merus*; *mel*=*melas*, *qua*=*quadriannulatus*. Arrows indicate introgression events.

## Interspecific introgression of 296G and 296S haplotypes

232 All four phylogenies exhibit two main clades separating *A. gambiae* and *A. coluzzii* haplotypes  
according to their 2La inversion karyotype, rather than by species (2La in blue, left; 2L<sup>+</sup><sup>a</sup> in red,  
234 right; ultrafast bootstrap support [UFBS] 91% and 97% respectively; Figure 6A). This clustering is  
due to the fact that the 2La inversion has been segregating in *A. gambiae* and *A. coluzzii* since  
236 before the beginning of their speciation (Fontaine et al. 2015).

A closer examination shows that *Rdl*-specific phylogenies (Figure 6A, B) have a distinct sub-clade  
238 within the 2La cluster, consisting of *A. coluzzii* 296S haplotypes and *A. arabiensis*, some of which  
also possess the 296S allele (light blue and green sequences in Figure in Figure 6A; UFBS 97%,  
240 84% for their sister-branch relationship). The deep branching of *A. arabiensis* haplotypes within  
the *A. gambiae/coluzzii* 2La clade is to be expected, as *A. arabiensis* 2La inversions descend from an  
242 ancient introgression event from the *A. gambiae/coluzzii* ancestor (Fontaine et al. 2015). However,  
their close phylogenetic relationship with *A. coluzzii* 296S haplotypes is suggestive of interspecific  
244 introgression.

To confirm this event of introgression and ascertain its direction, we compared the results of two  
246 complementary Patterson's *D* tests (Figure 7). The *D* statistic compares allele frequencies between  
three putatively admixing populations (A, B and C) and one outgroup (O), and can identify  
248 introgression between populations A and C (in which case  $D > 0$ ) or B and C ( $D < 0$ ; see Methods  
and (Durand et al. 2011; Patterson et al. 2012)).

250 Here, if 296S had emerged in *A. arabiensis* and later introgressed into *A. coluzzii*, we would expect  
296S *A. coluzzii* specimens to exhibit  $D > 0$  when compared to 296S *A. arabiensis*, but also to be  
252 more similar to *wt A. arabiensis* (from which 296S evolved) than to *wt A. coluzzii*. As predicted, we  
identify evidence of introgression between *A. coluzzii* 296S homozygotes and both (i) 296S *A.*  
254 *arabiensis* ( $D = 0.687 \pm 0.106$  standard error,  $p = 8.621 \times 10^{-11}$  derived from a *Z*-score  
distribution) and (ii) *wt A. arabiensis* ( $D = 0.506 \pm 0.123$ ,  $p = 3.959 \times 10^{-5}$ ; left panel in Figure 7A).  
256 Conversely, if 296S had introgressed from *A. coluzzii* into *A. arabiensis*, we would see evidence of  
introgression between 296S *A. arabiensis* and *wt A. coluzzii*, but we do not (right panel in Figure 7A;  
258  $D = -0.033 \pm 0.224$ ,  $p = 0.884$ ). These results are robust to various choices of outgroup species  
(*A. christyi* and *A. epiroticus*), and tests involving a negative control with fixed 2La inversions (*A.*  
260 *merus*) do not show evidence of introgression with 296S specimens (Supplementary Material  
SM12). Thus, we conclude that the 296S allele originated in *A. arabiensis* and later spread into *A.*  
262 *coluzzii*.

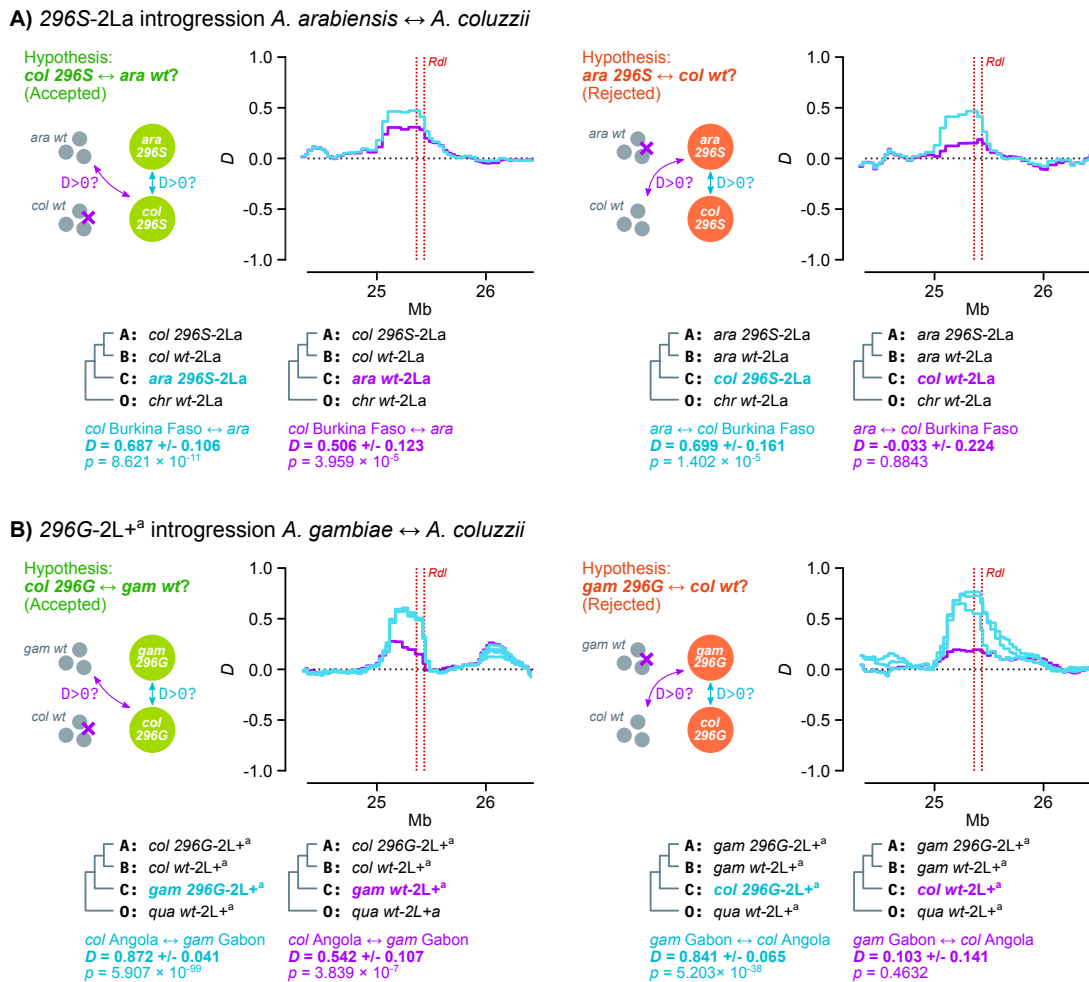


**Figure 7. Interspecific introgression. A)** Direction of 296S introgression between *A. arabiensis* and *A. coluzzii* (2La/2La background). We test two complementary hypothesis using Patterson’s *D* statistics: left, introgression between *A. coluzzii* 296S homozygotes (population A), *A. coluzzii* wt (B) and *A. arabiensis* (296S or wt; C) using *A. christyi* as outgroup (O); right, reversing the position of *A. coluzzii* and *A. arabiensis* as populations A/B and C. The complementary hypotheses can be summarised as follows: if 296S homozygotes from species *i* show evidence of introgression with wt homozygotes from species *j* (first test) but not with wt from species *i* (second test), 296S originated in species *j*. **B)** Direction of 296G introgression between *A. gambiae* and *A. coluzzii* (2L<sup>a</sup>/2L<sup>a</sup> background), testing two complementary hypothesis using Patterson’s *D* statistics: left, introgression between *A. coluzzii* 296G homozygotes (population A), *A. coluzzii* wt (B) and *A. gambiae* (296G or wt; C) using *A. quadriannulatus* as outgroup (O); right, reversing the position of *A. coluzzii* and *A. gambiae* as populations A/B and C. Color-coded cladograms at the bottom of each plot indicate the groups of specimens used in each test, including the average *D* in the *Rdl* locus with standard errors and *p*-values (estimated from the Z-score of jack-knifed estimates; see Methods). See detailed lists of comparisons and statistical analyses in Supplementary Material SM12 and SM13.

264 *Rdl* phylogenies (Figure 6A, B) also show a sub-clade of highly similar *A. gambiae* and *A. coluzzii*  
 haplotypes within the 2L<sup>a</sup> cluster, all of them carrying 296G alleles. This clade corresponds to the  
 266 swept haplotypes identified above (Figure 3). We established the polarity of introgression using  
 complementary Patterson’s *D* tests. Here, we found that 296G haplotypes from resistant *A. coluzzii*  
 268 populations (Côte d’Ivoire, Angola, and Ghana) exhibited signals of introgression with wt *A.*  
*gambiae* from Gabon (e.g.  $D = 0.542 \pm 0.107$ ,  $p = 3.839 \times 10^{-7}$  compared to Angolan *A. coluzzii*;

270 Figure 7B); but that this signal of introgression disappeared when comparing *wt A. coluzzii* to *296G*  
271 *A. gambiae* from Gabon (e.g.  $D = 0.103 \pm 0.141$ ,  $p = 0.4632$  compared to Angolan *A. coluzzii*;  
272 Figure 7B) or elsewhere (Supplementary Material SM13). These results support the introgression  
of *296G* from *A. gambiae* to *A. coluzzii*.

274 The fact that only Gabonese *A. gambiae* have significant support as the *296G* donor population  
could indicate that they are closer to the founding *296G* haplotype and/or the original  
276 introgression event. However, the negative results in other populations harbouring *296G* alleles  
(Cameroon, Guinea; Supplementary Material SM13) could also be due to methodological  
278 limitations of our analysis – e.g., our conservative approach is restricted to specimens that are  
homozygous for both the inversion karyotype ( $2L^{+a}/2L^{+a}$ ) and codon 296 (*296G/296G* or *wt/wt*);  
280 and the similarity between *wt A. gambiae* and *A. coluzzii* relative to the highly divergent swept  
haplotype can hinder the identification of the original background.

## 282 The *296G* haplotype spread from $2L^{+a}$ to $2La$ chromosomes

The haplotype phylogeny from the *Rdl* 3' region, where codon 296 variants reside, also revealed  
284 that the  $2L^{+a}$  clade (non-inverted, red; Figure 6A) contained a sub-cluster of *296G* haplotypes  
from both  $2L^{+a}$  (orange) and  $2La$  orientations (purple; Figure 6A; UFBS 98%). The deep branching  
286 of *296G-2La* haplotypes within the  $2L^{+a}$  clade implies that *296G* originated in a non-inverted  
background and later spread to inverted chromosomes via interkaryotypic introgression.  
288 Chromosomal inversions are strong barriers to recombination, but double cross-overs or gene  
conversion events can result in allelic exchange between non-concordant inversions (Andolfatto  
290 et al. 2001; Kirkpatrick 2010) and thus explain this phylogenetic arrangement.

However, the phylogeny of *Rdl* 5' haplotypes (which excludes codon 296 and the adjacent non-  
292 synonymous mutations) showed that *296G-2La* sequences (purple) branched within the *wt-2La*  
clade instead (blue; Figure 6B). Thus, interkaryotypic introgression only affects the swept  
294 haplotype at the 3' end of *Rdl* (Figures 3 and 4), whereas the 5' region is closer to the *wt*. We can  
confirm whether the introgression is specific to the 3' swept haplotype by examining the profile of  
296 sequence divergence along the *Rdl* gene locus (*Dxy*; Figure 8). We expect *296G* haplotypes to be  
more similar to *wt-2L<sup>+a</sup>* than to *wt-2La*, given that the *296G* allele first evolved in a  $2L^{+a}$   
298 background (blue line, *Dxy* ratio > 1; Figure 8). In the case of *296G* alleles from  $2La$  chromosomes,  
this expectation holds at the 3' region of *Rdl* but not at 5' nor outside of the gene, where allele  
300 frequencies are more similar to the *wt-2La* (purple line, *Dxy* ratio < 1; Figure 8).



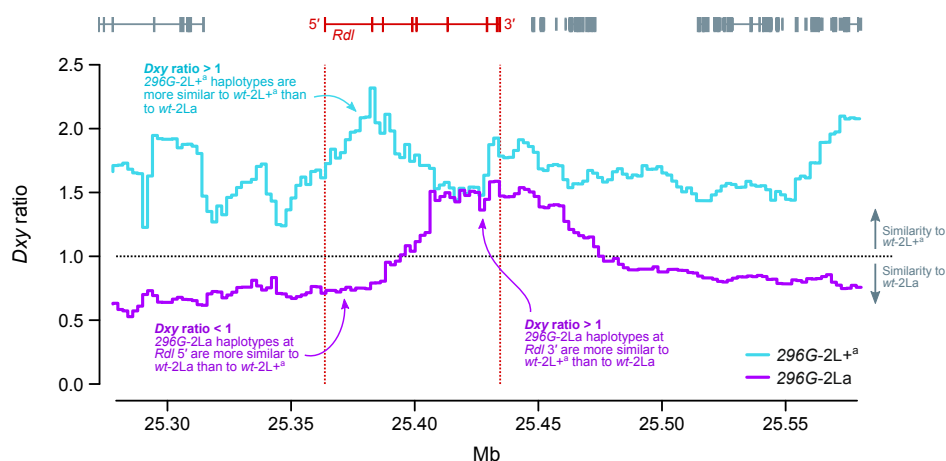


**Figure 8. Interkaryotypic introgression of 296G haplotypes.** Ratio of sequence divergence ( $D_{xy}$ ) between 296G and *wt* haplotypes of 2L+<sup>a</sup> and 2La origin. In this ratio, numerators are divergences between 296G haplotypes (of either 2L+<sup>a</sup> or 2La origin, in blue and purple respectively) relative to *wt*-2La haplotypes, and denominators are relative to *wt*-2L+<sup>a</sup>. Ratios >1 indicate similarity to *wt*-2L+<sup>a</sup>, and values <1 indicate similarity to *wt*-2La. All values are calculated in windows of 20,000 kbp with 10% overlap.

302 The presence of alleles from different karyotypic backgrounds in the 296G-2La *Rdl* sequences is  
 consistent with the sudden decay of haplotype homozygosity immediately upstream to codon 296  
 304 (Figure 4A), as the presence of *wt* alleles of 2La origin at 5' of the 296G swept haplotypes causes a  
 faster decay in haplotype homozygosity in 2La than in 2L+<sup>a</sup> haplotypes (Supplementary Material  
 306 SM14A). Concordantly, haplotype diversity at the 5' region of *Rdl* is higher in 296G-2La than in  
 296G-2L+<sup>a</sup> haplotypes (Supplementary Material SM14B).

### 308 **Structural modelling predicts that 296G and 296S disrupt the dieldrin binding site in alternative ways**

310 Finally, we investigated the effects of 296G and 296S resistance alleles on the structure of RDL  
 receptors. The *A. gambiae* RDL receptor was modelled as a homopentamer based on the human  
 312 GABA<sub>A</sub> receptor structure (Masiulis et al. 2019) (Figure 9). In *wt* receptors, the 296A residue is  
 located near the cytoplasmic end of the pore-lining second transmembrane helix (M2) and its  
 314 side chain is orientated into the pore (Figure 9A). Residue 345 is located distant from the pore, at  
 the cytoplasmic end of the M3 helix with its side chain orientated towards the lipid bilayer. We  
 316 carried out automated ligand docking for dieldrin in the *wt* receptor, finding a putative binding  
 site along the receptor pore where the insecticide docked with estimated free energy of binding  
 318 ( $\Delta G_b$ ) of -8.7 kcal/mol (Figure 9B). The 296A side chains form a major point of contact with the  
 ligand. A structure of human GABA<sub>A</sub> in complex with picrotoxin showed that this ligand forms



320 multiple hydrogen bonds with residues lining the pore (Masiulis et al. 2019), but dieldrin lacks  
equivalent hydrogen bond-forming groups. Thus, the close contacts between 296A side chains  
322 and dieldrin suggest that van der Waals interactions between these molecules are the  
predominant binding interaction.

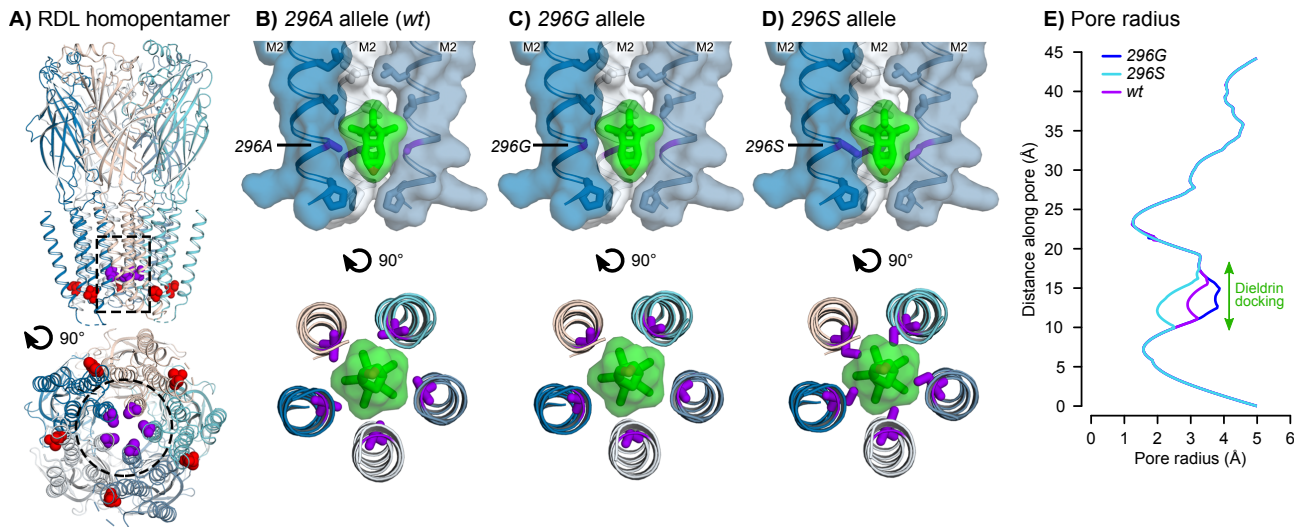


**Figure 9. RDL receptor models with docked dieldrin. A)** Homology model of the *A. gambiae* RDL homopentamer, viewed from the membrane plane (top) and cytoplasm (bottom). The 296A (purple) and 345T (red) positions are shown in space-fill. The dotted outlines depict the receptor regions in panels B-D. **B)** Docking prediction for dieldrin in the pore of the 296A (wt) receptor. Dielidrin is shown in green, in sticks and transparent surface. Side chains lining the pore are shown as sticks and 296A is coloured purple. **C-D)** Superimposition of dielidrin docking onto models of the 296G and 296S receptors, respectively. **E)** Pore radii in 296A, 296G and 296S models.

Next, we superimposed the wt dieldrin docking coordinates onto models of resistant RDL  
326 receptors, resulting in disruptions of the predicted form of interaction (Figure 9C, D). The A296G  
substitution widens the pore at the dieldrin docking site (2.9Å to 3.8Å) and reduces the surface  
328 area of contact between the lumen and dieldrin (Figure 9C, E). A296S has the opposite effect: it  
results in a narrower pore (2Å) and shows an overlap between the serine side-chains and dieldrin,  
330 which indicates that steric hindrance could prevent the insecticide from binding at this location  
(Figure 9D, E).

332

## Discussion

### 334 Evolution of *Rdl* resistance: selective sweeps and multiple introgression events

336 Contemporary dieldrin-resistant *A. gambiae* and *A. coluzzii* appear to descend from two unique hard selective sweeps linked to the *A296G* and *A296S* mutations, respectively (Figures 3 and 4).  
338 Both sweeps occurred independently on different genomic backgrounds (Figure 6), and have undergone at least three introgression events (Figures 6-8): (i) *296G* from *A. gambiae* to *A. coluzzii*;  
340 (ii) *296G* from 2L+<sup>a</sup> to 2La chromosomes; and (iii) *296S* from *A. arabiensis* to *A. coluzzii*.

In the case of *296G*, our data supports an origin in *A. gambiae* with 2L+<sup>a</sup> chromosomes, followed by  
342 interspecific introgression into *A. coluzzii*, and interkaryotypic introgression into 2La chromosomes. The *A. gambiae* origin is inferred from the background similarity between *A.*  
344 *coluzzii* swept haplotypes and *A. gambiae wt* specimens from Gabon (according to Patterson's *D* test; Figure 7B). *A. gambiae* resistance haplotypes have accrued more non-synonymous mutations  
346 than *A. coluzzii* (*N530K* and *H539Q*; Figure 1A), which is consistent with a longer evolutionary history in the former. In either case, the swept haplotype currently spans populations of both  
348 species across West and Central Africa – mimicking the pan-African selective sweep described for the homologous *Rdl* mutation in *D. melanogaster* (ffrench-Constant, Rocheleau, et al. 1993; ffrench-  
350 Constant, Steichen, et al. 1993; Thompson et al. 1993). This result is in line with previous studies that had hypothesized the existence of a pan-African *296G* sweep due to the strong genetic  
352 differentiation found in this locus (Lawniczak et al. 2010).

The interkaryotypic introgression of *296G* haplotypes from non-inverted 2L+<sup>a</sup> into 2La  
354 chromosomes (Figures 6 and 7) also facilitated the spread of *296G* resistance alleles, e.g. in *A. gambiae* populations with high frequencies of 2La/2La karyotypes such as Burkina Faso (Figure  
356 5C). This introgression event affected a short region around codon 296 at the 3' end of *Rdl*, which contributes to the faster decay in haplotype homozygosity immediately upstream to the  
358 resistance mutations (Figure 4A and Supplementary Material SM14A). While it is generally acknowledged that chromosomal inversions strongly suppress recombination (Sturtevant 1917),  
360 genetic exchange can occur via double cross-over recombination or gene conversion (Chovnick 1973; Rozas and Aguadé 1994; Andolfatto et al. 2001; Kirkpatrick 2010). The reduction in  
362 recombination is weaker in regions distant from the inversion breakpoints (Andolfatto et al. 2001), as it is the case for *Rdl* (located ~4.8 Mb and ~16.7 Mb away from the 2La breakpoints),  
364 which results in reduced differentiation at the centre of the inversion (Stump et al. 2007; Cheng et

al. 2012) (Supplementary Material SM15). To the best of our knowledge, reports of adaptive  
366 introgression of individual genes within inversions are rare. In *Anopheles*, one of such cases are  
certain loci involved in adaptation to desiccation, which are linked to 2La inversions but are  
368 exchanged in 2La/2L<sup>a</sup> heterozygotes (Cheng et al. 2012; Ayala et al. 2019). Another example,  
possibly linked to gene conversion, could be the *APL1* cluster of hyper-variable immune genes:  
370 their pattern of sequence variation is more strongly influenced by geography and species (*A.*  
*gambiae/A. coluzzii*) than by the 2La inversion where they reside (Rottschaefer et al. 2011).

372 On the other hand, the *296S* selective sweep has a more restricted geographical distribution. In  
the *Ag1000G* cohort, *296S* is only found in *A. coluzzii* from Burkina Faso (Figure 3). We also identify  
374 *296S* alleles in *A. arabiensis* specimens from East (Tanzania), Central (Cameroon) and West Africa  
(Burkina Faso); as well as two *A. quadriannulatus* specimens from Zambia (which appears to be the  
376 first record in this species; Figure 1B).

Interestingly, we find clear evidence of *296S* introgression from *A. arabiensis* into *A. coluzzii* even  
378 when comparing to *A. arabiensis wt* specimens (Figure 7A), and despite the fact that none of the *A.*  
*arabiensis 296S* share the *A. coluzzii* swept haplotype (Figures 3A, 6A, and Supplementary Material  
380 SM6). Thus, lack of genomic evidence from *A. arabiensis* precludes the identification of the actual  
donor haplotype. A wider sampling of *A. arabiensis* populations will be necessary to complete the  
382 picture of *296S* evolution, in order to (i) identify the number of historical *A296S* mutations in this  
species; (ii) establish whether they were associated with one or more selective sweeps; and (iii)  
384 whether any of these hypothetical sweeps introgressed into *A. coluzzii*.

### **Persistence of *Rdl* mutations after dieldrin withdrawal**

386 *Rdl* is a highly conserved gene, with an extreme paucity of non-synonymous mutations over >100  
Mya of evolutionary divergence (Neafsey et al. 2015) in culicines and anophelines, and low  $d_N/d_S$   
388 ratios that indicate a prevalence of purifying selection (Supplementary Material SM4). In this  
context, the persistence of *296G* and *296S* alleles in natural populations for more than 70 years, in  
390 spite of its fitness costs in the absence of insecticide (Rowland 1991a; Rowland 1991b; Platt et al.  
2015), has been a long-standing puzzle.

392 Our study provides two key insights to this question. First, we find that, relative to the *wt*,  
haplotypes with resistance alleles have an excess of non-synonymous genetic diversity (~18x  
394 increase in  $\pi_N/\pi_S$  in *296G*, ~4x in *296S*). This observation suggests that the emergence of *296G* and,  
to a lesser degree, *296S*, has substantially altered the selective regime of *Rdl* and enabled the  
396 accumulation of additional non-synonymous mutations in an otherwise highly constrained

protein. This accelerated rate of protein evolution appears to have occurred in the only copy of  
398 the resistance haplotype, as there is no evidence of copy number variation polymorphisms  
affecting *Rdl* in the *Ag1000G* dataset (Lucas et al. 2019; The *Anopheles gambiae* 1000 Genomes  
400 Consortium 2019). A similar change has been recently observed for resistance mutations in *Vgsc*  
(the target site of pyrethroids), whereby *995F* haplotypes accumulate an excess of amino-acidic  
402 substitutions (Clarkson et al. 2018).

Second, we identify a high degree of genetic linkage between the *296G/345M* and *296S/345S* allele  
404 pairs, which is observed in all West African populations where codon 296 mutations are present  
(Figures 1, 2, and Supplementary Material SM3) due to the fact that virtually all swept haplotypes  
406 include both mutations (Figures 3 and 4). This near-universal association is highly relevant  
because codon 345 mutations are suspected to have compensatory effects that offset the costs of  
408 codon 296 variants (Remnant et al. 2014; Taylor-Wells et al. 2015). Studies of fipronil resistance  
have shown that both the *296G* allele and the combination of *296G* and *345M* alleles resulted in  
410 decreased insecticide sensitivity in *A. gambiae* (Taylor-Wells et al. 2015), *D. melanogaster* (Remnant  
et al. 2014), and *D. simulans* (Le Goff et al. 2005). Crucially, Taylor-Wells *et al.* (Taylor-Wells et al.  
412 2015) showed that, in addition to fipronil resistance, the *A. gambiae 296G* allele causes heightened  
sensitivity to the GABA neurotransmitter (possibly contributing to the observed fitness costs  
414 (Rowland 1991b; Rowland 1991a; Platt et al. 2015)); and that the addition of the *345M* mutation  
reduces these detrimental effects while still conferring resistance.

416 Interestingly, our structural modelling analyses predict opposite resistance mechanisms for each  
resistance allele: *296G* results in a wider RDL pore with reduced van der Waals interactions with  
418 dieldrin (Figure 9C, E); whereas *296S* narrows the pore and impedes dieldrin docking due to steric  
hindrance (Figure 9D, E). These two effects suggest the possibility that the mechanisms behind  
420 the hypothesised compensatory roles of codon 345 mutations could be different as well, and open  
a new line of inquiry to investigate the exclusive association of each resistance variant with  
422 downstream mutations (*296G* with *345M*, *296S* with *345S*). Yet, the exact nature of the interaction  
between these codon 296 and 345 mutations remains unclear. Firstly, residue 345 does not have  
424 direct contacts with dieldrin or residue 296 (Figure 9A), and changes on its side chain do not  
directly affect the pore conformation. Secondly, indirect effects are uncertain too: in human  
426 receptors, mutations at the interface between the third and second transmembrane helices  
(where residues 345 and 296 reside, respectively) affect the transition to the desensitized  
428 functional state (Gielen et al. 2015); but residue 345 in *A. gambiae* is not buried in this interface  
and is instead facing the lipid bilayer (Figure 9A), and the predicted effects of mutations *T345M*

430 and *T345S* are not obvious.

Other possible factors behind the persistence of *Rdl* resistance alleles include the long half-life of  
432 dieldrin as an environmental organic pollutant; as well as the fact that it is the target site of  
insecticides other than dieldrin. The use of fipronil as a pesticide has been proposed to explain  
434 the high frequencies of *Rdl* mutations after dieldrin withdrawal from specific sites (Wondji et al.  
2011; Kwiatkowska et al. 2013), e.g. in *A. coluzzii* from the Vallée du Kou (Burkina Faso)  
436 (Kwiatkowska et al. 2013). Neonicotinoids (imidacloprid) and pyrethroids (deltamethrin) could  
also contribute to *Rdl* mutation maintenance, as they interact with *Rdl* as a secondary target when  
438 used at high concentrations (Taylor-Wells et al. 2015). Pyrethroids have been a major vector  
control tool across most of sub-Saharan Africa (van den Berg et al. 2012; Oxborough 2016) in the  
440 years prior the collection of the samples used in this study (up to 2012). Finally, other drugs  
known to interact with *Rdl* have a less clear possible connection with the persistence of the *296G*  
442 or *296S* alleles. For example, isoxazolines and meta-diamides are still effective in the presence of  
codon 296 mutations (Ozoe et al. 2010; Nakao et al. 2013; Asahi et al. 2015), which suggests that  
444 they are unlikely to be a primary cause of the maintenance of these alleles in natural populations.  
*Rdl* is also a secondary target of ivermectin (Chaccour et al. 2013). This drug does not bind in  
446 proximity to codon 296, but the *296S* allele nevertheless appears to reduce ivermectin interaction  
with an *in vitro*-expressed GABA receptors in *Drosophila* (Nakao et al. 2015). Ivermectin was  
448 introduced into mass drug administration campaigns in the 1990s, first for onchocerciasis, then  
lymphatic filariasis (Hoerauf et al. 2011). Whilst the interaction of ivermectin with *Rdl* resistance  
450 alleles *in vivo* is not currently understood, these mutations have persisted for two decades  
between the discontinuation of cyclodiene use and the first mass ivermectin administration  
452 campaigns.

### Implications for vector control

454 The apparent ease with which *Rdl* adaptive haplotypes have spread across the barriers to  
recombination posed by species isolation (*A. gambiae*/*A. coluzzii* and *A. arabiensis*/*A. coluzzii*) and  
456 non-concordant chromosomal inversions (2L<sup>+</sup>/2La) mirrors previous findings in *Vgsc* target site  
mutations (Clarkson et al. 2014), and suggests worrying consequences for insecticide deployment  
458 programmes. Burkina Faso, where resistance alleles have traversed both barriers to  
recombination, is a case-in-point example of this risk: the high frequency of 2La inversions  
460 (Figure 5C) did not prevent the spread of *296G*, and interspecific introgression of *296S* from *A.*  
*arabiensis* compounded this problem in *A. coluzzii*.

462 Also noteworthy is the overlap of *Rdl* and *Vgsc* resistance variants in West and Central Africa. The  
lack of genetic linkage between *Vgsc* and *Rdl* resistance haplotypes suggests that this co-  
464 occurrence is purely geographical, and does not fit a hypothetical epistatic relationship  
(Supplementary Material SM7 and SM8). Yet, this overlap is still relevant for vector control: as  
466 pyrethroid resistance increases in *Anopheles* populations (Ranson et al. 2011), the search for  
substitutes should take into account that some can be rendered ineffective by *296S* or *296G* (e.g.  
468 fipronil (Gant et al. 1998), ivermectin (Miglianico et al. 2018), or, possibly, neonicotinoids such as  
imidacloprid (Taylor-Wells et al. 2015)). This risk is currently highest in the West and Central  
470 African populations of *A. gambiae* and *A. coluzzii* where both *296G* and *Vgsc 995F* (Clarkson et al.  
2018) are common (Supplementary Material SM8). In the future, the introgression of *296S* from  
472 East African *A. arabiensis* could further compound current complications caused by the already  
high frequencies of *Vgsc 995S* in this region (Clarkson et al. 2018).

474 This case study of the mechanisms that underlie persistence of dieldrin resistance is also relevant  
for integrated resistance management. Strategies such as insecticide rotations or mosaics rely on  
476 a gradual decline in resistance over time (World Health Organization 2012). Instead, *296G* and  
*296S* haplotypes have accumulated additional non-synonymous mutations (Figure 3A), some of  
478 which (codon 345) are putatively compensatory. As mentioned above, a similar altered selective  
regime has also been observed in *Vgsc* haplotypes with *kdr* mutations (Clarkson et al. 2018).  
480 Interestingly, a study of Brazilian *Aedes aegypti* found that *Vgsc kdr* mutations did not decrease in  
frequency after a decade without public pyrethroid spraying campaigns (Macoris et al. 2018).  
482 Brazilian *Aedes* have a longer history of pyrethroid-based treatments than African *Anopheles spp.*  
(van den Berg et al. 2012; Macoris et al. 2018); thus, their resilient *kdr* mutations could be (i)  
484 recapitulating our observations with respect to *Rdl* and dieldrin, and (ii) prefiguring a similar  
persistence of *Vgsc kdr* in the *A. gambiae* complex after a future phasing-out of pyrethroids in  
486 response to their decreasing efficacy (Ranson et al. 2011).

Overall, our results show that the *Rdl* resistance mutations that appeared after the pioneering  
488 deployment of dieldrin in the 1950s will still be relevant in the immediate future. Continued  
monitoring is thus necessary to understand the evolving landscape of genomic variation that  
490 underlines new and old mechanisms of insecticide resistance.

# Methods

## 492 Data collection

We used genome variation data from *A. coluzzii* and *A. gambiae* mosquitoes from the *Anopheles*  
494 *gambiae* 1000 Genomes Phase 2-AR1. This dataset consists of 1,142 wild-caught mosquitoes  
(1,058 females and 84 males) from 33 sampling sites located in 13 sub-Saharan African countries  
496 (Supplementary Material SM1). To ensure population representativeness, The *Anopheles gambiae*  
1000 Genomes Consortium aimed at minimum sample size of 30 specimens per country (Miles et al.  
498 al. 2017) and avoided confounding factors during collection (e.g. insecticide resistance). The list  
of locations includes continental and island populations, and covers different ecosystems  
500 (including rainforest, coastal forests, savannah, woodlands, and grasslands; details in (Miles et al.  
2017; The *Anopheles gambiae* 1000 Genomes Consortium 2019)). Specimens were collected at  
502 different times between 2009 and 2012 (with the exception of samples from Gabon and  
Equatorial Guinea, collected in 2000 and 2002 respectively).

504 The methods for genome sequencing and analysis of this dataset have been previously described  
in detail as part of the Phase 1 and Phase 2 releases of *Ag1000G* (Miles et al. 2017; The *Anopheles*  
506 *gambiae* 1000 Genomes Consortium 2019). Briefly, DNA was extracted from each of the 1,142  
mosquitoes using Qiagen DNeasy Blood and Tissue Kit (Qiagen Science, US) and sequenced with  
508 the Illumina HiSeq 2000 platform (Wellcome Sanger Institute, UK) using paired-end libraries  
(100 bp reads with insert sizes in the 100-200 bp range) and aiming at a 30x coverage per  
510 specimen (see original papers for details). Variant calling was performed using *bwa* 0.6.2 (Li and  
Durbin 2009) and the *GATK* 2.7.4 *UnifiedGenotyper* module (Van der Auwera et al. 2013). Haplotype  
512 phasing was estimated with *SHAPEIT2* (Delaneau et al. 2013), and variant effects were predicted  
using *SnPEff* 4.1b (Cingolani et al. 2012).

514 We retrieved the phased genotype calls, SNP effect predictions, and the array of accessible  
genomic positions for each of the 1,142 specimens from the *Ag1000G* Phase 2-AR1 online archive  
516 (The *Anopheles gambiae* 1000 Genomes Consortium 2017). We also obtained the same data for  
populations of four species in the *Anopheles* complex (*A. arabiensis*, *A. quadriannulatus*, *A. melas* and  
518 *A. merus*) and two outgroups (*A. epiroticus* and *A. christyi*) (Neafsey et al. 2015), as available in the  
*Ag1000G* online archive (The *Anopheles gambiae* 1000 Genomes Consortium 2017). The complete  
520 list of genomes with accession codes is available in Supplementary Material SM1.

The reference gene annotation of *A. gambiae* was obtained from Vectorbase (Giraldo-Calderón et

522 al. 2015) (GFF format, version AgamP4.9). Gene and variant coordinates employed in this study  
are based on the AgamP4 version of the genome assembly.

## 524 **Genotype frequencies and linkage disequilibrium**

We retrieved all non-synonymous genomic variants located within the coding region of *Rdl*  
526 (genomic coordinates: 2L:25363652-25434556) that were biallelic, phased, and segregating at  
>5% frequency in at least one population (henceforth, ‘non-synonymous variants’). Parsing and  
528 filtering of genotype calls from *Ag1000G* was done using the *scikit-allele* 1.2.1 library (Miles and  
Harding 2017) in Python 3.7.4.

530 We calculated the linkage disequilibrium between each pair of non-synonymous variants using (i)  
Rogers’ and Huff *r* correlation statistic (Rogers and Huff 2009), as implemented in *scikit-allele*  
532 (*rogers\_huff\_r*); and (ii) Lewontin’s *D'* statistic (Lewontin 1964), as implemented in (Clarkson et al.  
2018).

## 534 **Haplotype networks**

We constructed a network of haplotype similarity using 626 biallelic, phased and non-singleton  
536 (shared between more than two samples) variants located in a region  $\pm$  10kbp of *Rdl* codon 296  
(middle nucleotide, coordinate 2L:25429236). We used the presence/absence of each allele within  
538 this genomic region to calculate Hamming distances and build minimum spanning networks  
(Bandelt et al. 1999), using the *hapclust* function from (Clarkson et al. 2018) (with distance breaks  
540 >3 variants). Network visualizations were produced using the *graphviz* 2.38.0 Python library  
(Ellson et al.), with haplotype clusters being color-coded according to species, population and  
542 presence/absence of the resistance alleles in codon 296 (*296S*, 2L:25429235; *296G*, 2L:25429236)  
and the 995th codon of *Vgsc* (Figure 3, Supplementary Material SM5, and SM6). The network  
544 visualization in Figure 3A excludes singletons and haplotype clusters with a cohort frequency  
<1%.

546 We calculated the sequence diversity ( $\pi$ ) of each haplotype group in the same region  
(*sequence\_diversity* function in *scikit-allele*), using a jack-knife procedure (iterative removal of  
548 individual haplotypes without replacement) (Tukey 1958) to estimate the average and standard  
error. We also calculated the sequence diversity in non-synonymous coding variants from this  
550 region ( $\pi_N$ ), synonymous coding variants ( $\pi_S$ ), and their ratio ( $\pi_N/\pi_S$ ).

## **Positive selection in haplotype clusters**



552 We analysed the signals of positive selection in three haplotype groups, divided according to  
alleles in codon 296: *wt* ( $n = 1476$ ), *296S* ( $n = 94$ ) and *296G* ( $n = 651$ ) (Supplementary Material  
554 SM5). First, we calculated the extended haplotype homozygosity decay (*EHH*) of each group of  
haplotypes, using 22,910 variants (phased and biallelic) located  $\pm 200$  kbp of codon 296  
556 (2L:25429236) (using the *ehh\_decay* utility in *scikit-allel*). For each haplotype group, we recorded  
the genomic region where *EHH* decay  $>0.95$  and  $<0.05$ .

558 Second, we calculated the profile of Garud's *H* statistics (Garud et al. 2015) along the 2L  
chromosomal arm (*moving\_garud\_h* utility in *scikit-allel*; block length = 500 phased variants with  
560 20% step). We performed the same calculations for the haplotypic diversity  
(*moving\_haplotype\_diversity* in *scikit-allel*). We calculated the Garud *H* and haplotypic diversity  
562 estimates in the *Rdl* locus, using a jack-knife procedure (Tukey 1958) (iterative removal of  
individual haplotypes without replacement) to calculate the mean and standard error of each  
564 statistic.

## Karyotyping of 2La inversions

566 In order to assign karyotypes of the 2La inversion in all specimens from *Ag1000G* Phase 2, we  
used known 2La karyotypes from Phase 1 as a reference (Miles et al. 2017), and analysed  
568 genotype frequencies within the inversion by principal component analysis (PCA). Specifically, we  
retrieved the genotype frequencies of 1142 specimens from *Ag1000G* Phase 2, 765 of which were  
570 also present in Phase 1 and had been previously karyotyped for this inversion (Miles et al. 2017);  
and selected 10,000 random SNPs (biallelic, shared between more than two samples, phased,  
572 segregating in at least one population, and located within the 2La inversion 2L:20524058-  
42165532). SNPs fitting these criteria were selected using the *scikit-allel* Python library, and the  
574 PCA was performed using the *randomized\_pca* utility (with Patterson scaling).

Manual inspection of the principal components (Supplementary Material SM9) showed that PC1  
576 (6.35% of variance explained) was sufficient to discriminate between known karyotypes from  
Phase 1 using a clear-cut threshold (2La/2La, 2La/2L<sup>+a</sup> and 2L<sup>+a</sup>/2L<sup>+a</sup>). We determined the  
578 optimal classification thresholds using the C-Support Vector classification method (SVC, a method  
for supervised learning) implemented in the *scikit-learn* 0.21.3 Python library (Pedregosa et al.  
580 2011). Specifically, we used the *SVC* function in *scikit-learn* (*svm* submodule) to train a classifier  
with known karyotypes from Phase 1 (765 observations) and the main principal components of  
582 the PCA analysis (10 variables), using a linear kernel and  $C=1$ . The selected thresholds were able  
to classify Phase 1 data into each of the three categories (2La/2La, 2La/2L<sup>+a</sup> and 2L<sup>+a</sup>/2L<sup>+a</sup>) with

584 100% accuracy (as per the classifier *score* value), precision and recall (calculated using the  
585 *classification\_report* function from the *scikit-learn metrics* submodule).

## 586 **Phylogenetic analysis of haplotypes**

We obtained genomic alignments of SNPs located from four regions around the *Rdl* locus, at the  
588 following coordinates: (i) 5' start of the gene (2L:25363652 +/- 10,000 kbp, 696 variants), (ii) 3'  
589 end of the gene (2L:25434556 +/- 10,000 kbp, 428 variants), (iii) unadmixed region 1Mb  
590 upstream of *Rdl* (2L:24363652 + 20,000 kbp; 2903 variants; inside of the 2La inversion), and (iv)  
591 unadmixed region 1Mb downstream of *Rdl* (2L:26434556 + 20,000 kbp, 2594 variants; inside of  
592 the 2La inversion). These alignments were built from phased, biallelic variants within the  
aforementioned regions, obtained from *A. coluzzii* and *A. gambiae* (*Ag1000G* Phase 2), *A. arabiensis*,  
594 *A. quadriannulatus*, *A. melas* and *A. merus*. We restricted our analysis to haplotypes pertaining to  
individuals homozygous for the 2La inversion (2La/2La and 2L<sup>+</sup><sup>a</sup>/2L<sup>+</sup><sup>a</sup>), totalling 1684 haplotypes  
596 (out of 2356 haplotypes in the original dataset, obtained from 1178 specimens). Invariant sites  
were removed from the alignments using *snp-sites* 2.3.3 (Page et al. 2016). All alignments are  
598 available in Supplementary Material SM10.

Each genomic alignment was then used to compute Maximum-Likelihood phylogenetic trees  
600 using *IQ-TREE* 1.6.10 (Nguyen et al. 2015). The best-fitting nucleotide substitution model for each  
alignment was selected using the *TEST* option of *IQ-TREE* and according to the Bayesian  
602 Information Criterion (BIC), which suggested the GTR substitution matrix with ascertainment  
bias correction, four gamma ( $\Gamma$ ) rate categories, and empirical state frequencies observed from  
604 the alignment (F) (i.e. the *GTR+F+ASC+G4* model in *IQ-TREE*). We calculated branch statistical  
supports using the UF bootstrap procedure (Minh et al. 2013; Hoang et al. 2018) and refined the  
606 tree for up to 10,000 iterations, until convergence was achieved (correlation coefficient  $\geq 0.99$ ).

Tree visualizations were created in R, using the *plot.phylo* function from the *ape* 5.3 library  
608 (Paradis and Schliep 2019) and *stringr* 1.4.0 (Wickham 2019). Each phylogeny was midpoint-  
rooted with *phytools* 0.6-60 (Revell 2012) (*midpoint.root*), and branch lengths in Figure 6 were  
610 constrained for display purposes ( $5 \times 10^{-5}$  to  $5 \times 10^{-3}$  per-base substitutions range; unmodified  
trees available in Supplementary Material SM11).

## 612 **Interspecific introgression with Patterson's *D* statistic**

We analysed the signals of introgression along the 2L chromosomal arm using Patterson's *D*  
614 statistic (Durand et al. 2011; Patterson et al. 2012). This statistic requires allele frequencies in

four populations (A, B, C and O) following a predefined (((A,B),C),O) phylogeny, where A, B and C  
616 are populations with possible introgression events, and O is an unadmixed outgroup. Then,  $D > 0$   
if there is an excess of allele frequency similarities between A and C (which means either  $A \rightarrow C$  or  
618  $C \rightarrow A$  introgression) and  $D < 0$  for excess of similarity between B and C ( $B \rightarrow C$  or  $C \rightarrow B$   
introgression) (Durand et al. 2011; Patterson et al. 2012). We calculated Patterson's  $D$  along blocks  
620 of adjacent variants in the 2L chromosomal arm (block length = 10,000 variants, with 20% step  
length; phased variants only) using the *moving\_patterson\_d* utility in *scikit-allel*. We also calculated  
622  $D$  in the *Rdl* locus (2L:25363652-25434556), and estimated its deviation from the null expectation  
(no introgression:  $D = 0$ ) with a block-jackknife procedure (block length = 100 variants;  
624 *average\_patterson\_d* in *scikit-allel*). We then used these jack-knifed estimates to calculate the  
standard error,  $Z$ -score and the corresponding  $p$  value from the two-sided  $Z$ -score distribution.

626 Using the procedure described above, we performed multiple analyses of introgression between  
combinations of populations fitting the (((A,B),C),O) phylogeny. For each analysis, we selected A, B,  
628 C and O populations according to two criteria: (i) which interspecific introgression event was  
under test (*A. gambiae* ~ *A. coluzzii* or *A. coluzzii* ~ *A. arabiensis*); (ii) homozygous karyotypes of the  
630 2La inversion within which *Rdl* is located (given that it introduces a strong effect on genotype  
frequencies across the entire *A. gambiae* species complex (Fontaine et al. 2015)) and the  
632 resistance haplotype in question; and (iii) exclude populations with high frequencies of hybrids,  
with controversial species identification, or with extreme demographic histories (Guinea-Bissau,  
634 The Gambia, and Kenya) (Miles et al. 2017; Vicente et al. 2017). Following these criteria, we then  
tested the presence and direction introgression between the combinations of populations  
636 specified below.

First, we tested the *A. coluzzii* ~ *A. arabiensis* introgression of the *296S* haplotype in inverted  
638 genomes (2La/2La homozygotes; Figure 7A and Supplementary Material SM12). We performed  
two versions of this test, using either *A. coluzzii* or *A. arabiensis* as donors (population C), which can  
640 give an indication of the population of origin of the *296S* mutation. First, we tested the *A. arabiensis*  
 $\rightarrow$  *A. coluzzii* hypothesis using: (i) *296S* homozygous *A. coluzzii* from Burkina Faso as population A;  
642 (ii) *wt* homozygous *A. coluzzii* from Burkina Faso as population B; (iii) *A. arabiensis* and *A. merus*  
specimens as multiple C populations (donors) C, treating *296S* and *wt* homozygous specimens as  
644 different populations; and (iv) *A. epiroticus* and *A. christyi* as population O. Second, we tested the *A.*  
*coluzzii*  $\rightarrow$  *A. arabiensis* hypothesis but switching the position of *A. arabiensis* (now population A and  
646 B, for *296S* and *wt* respectively) and *A. coluzzii* populations (now population C, together with the *A.*  
*merus* negative control). Under this setup, we expect to see evidence of introgression between

648 *296S A. coluzzii* and *296S A. arabiensis* in both tests (positive controls), but a positive result with any  
of the *wt* comparisons can indicate that *296S* haplotypes in either species is more similar to *wt*  
650 from the other (and hence, the second species is the species of origin). A detailed account of all  
comparisons, populations and complete statistical reports are available in Supplementary  
652 Material SM12.

We performed the same series of tests for the *A. gambiae* ~ *A. coluzzii* introgression of the *296G*  
654 cluster in individuals without the 2La inversion ( $2L^{+a}/2L^{+a}$  homozygotes; Figure 7B and  
Supplementary Material SM13A, B) and with the 2La inversion (Supplementary Material SM13C,  
656 D). In these tests, homozygous individuals from various *A. gambiae* and *A. coluzzii* populations  
were alternatively used as groups A/B (A if *296G*, B if *wt*) and C (*296G* and *wt*, separately); and *wt*  
658 outgroups were selected according to their 2La karyotype ( $2L^{+a}/2L^{+a}$ : *A. quadriannulatus* and *A.*  
*melas*;  $2La/2La$ : *A. merus*). A detailed account of all comparisons, populations and complete  
660 statistical reports are available in Supplementary Material SM13.

### Sequence divergence between 2La karyotypes

662 To ascertain whether *296G* karyotypes from 2La chromosomes were introgressed from a  $2L^{+a}$   
background, we calculated the absolute sequence divergence (*Dxy* (Takahata and Nei 1985))  
664 around the *Rdl* locus between all combinations of the following groups of haplotypes: (i) between  
*296G*-carrying haplotypes from  $2L^{+a}/2L^{+a}$  homozygotic genomes, (ii) *wt* haplotypes from  $2La/2La$ ;  
666 (iii) *296G* haplotypes from  $2La/2La$ , (iv) *wt* haplotypes from  $2La/2La$  (Figure 8). *Dxy* estimates were  
calculated along the 2L arm using the *windowed\_divergence* utility in *scikit-allel* (window  
668 size=20,000 bp with 10% overlap). At each window, we also calculated the ratio between the  
following *Dxy* estimates: (i)  $296G-2L^{+a} \sim wt-2La / 296G-2L^{+a} \sim wt-2L^{+a}$ ; and (ii)  $296G-2La \sim wt-2La /$   
670  $296G-2La \sim wt-2L^{+a}$ . Thus, windows with ratios >1 are more similar to the *wt-2L<sup>+</sup>a* background,  
and windows with ratios <1 are more similar to the *wt-2La* background.

### 672 Alignment of *Rdl* orthologs

We retrieved *Rdl* orthologs from the following species of the Culicidae family (available in  
674 Vectorbase): *A. gambiae*, *A. arabiensis*, *A. melas*, *A. merus*, *A. christyi*, *A. epiroticus*, *A. minimus*, *A.*  
*culicifacies*, *A. funestus*, *A. stephensi*, *A. maculatus*, *A. farauti*, *A. dirus*, *A. atroparvus*, *A. sinensis*, *A.*  
676 *albimanus*, *A. darlingi*, *Aedes aegypti*, *Aedes albopictus*, and *Culex quinquefasciatus*. We retained (i)  
those orthologs that resulted in complete predicted peptides (defined as having the same start  
678 and end codons as the *A. gambiae Rdl*), and (ii) the longest isoform per gene (except for *A. gambiae*,  
where all three isoforms were retained). These sequences were aligned using *MAFFT* 7.310 (1,000

680 rounds of iterative refinement, G-INS-i algorithm) (Kato and Standley 2013). Pairwise sequence  
identity between peptide sequences was calculated using the *dist.alignment* function (with a  
682 identity distance matrix, which was then converted to a pairwise identities) from the *seqinr* 3.4-5  
library (Charif and Lobry 2007), in R 3.6.1 (R Core Team 2017). Pairwise  $d_N/d_S$  ratios were  
684 calculated from a codon-aware alignment of CDS sequences, using the *dnds* function from the *ape*  
5.3 R library (Paradis et al. 2004). The codon-aware alignment of full-length CDS was obtained  
686 with PAL2NAL (Suyama et al. 2006), using the peptide alignment as a reference. Tables of  
pairwise identity and  $d_N/d_S$  values have been created with *heatmap* 1.0.12 (Kolde 2019).

## 688 **Homology modelling and automated ligand docking**

The structure of human GABA<sub>A</sub> receptor bound with picrotoxin (PDB accession: 6HUG) provided  
690 the template for generating a homology model of the homopentameric *A. gambiae* RDL receptor  
(UniProtKB accession: Q7PII2). Sequences were aligned using *Clustal Omega* (Sievers et al. 2011),  
692 and 50 homology models were generated using *MODELLER* 9.23 (Eswar et al. 2006). A single best  
model was chosen based on the internal scoring values from *MODELLER* and by visually  
694 inspecting models in *Swiss-PdbViewer* (Guex et al. 1999) to eliminate candidates with structural  
problems. The *A296G* and *A296S* mutants were generated using *Swiss-PdbViewer* to introduce the  
696 amino acid substitutions and to energy minimise the resulting structures using 50 steps of  
conjugate gradient energy minimization. The pore radii of the channel models were calculated  
698 using *HOLE* 2.0 (Smart et al. 1996). The 3-dimensional structure of dieldrin was generated ab  
initio using *MarvinSketch* 19.22 of the ChemAxon suite (ChemAxon 2019). *AutoDockTools* 1.5.6  
700 (Morris et al. 2009) was used to define rotatable bonds and merge non-polar hydrogens.

Automated ligand docking studies with the wild-type GABA receptor model were performed using  
702 *AutoDock Vina* 1.1.2 (Trott and Olson 2009) with a grid of 20 × 20 × 20 points (1Å spacing) centred  
on the channel pore. Figures were produced using *PyMOL* (Schrödinger 2015).

## 704 **Availability of code and data**

Python (3.7.4) and R scripts (3.6.1) to reproduce all analyses in this manuscript are available on  
706 GitHub: <https://github.com/xgrau/rdl-Agam-evolution>

All genome variation data has been obtained from the publicly available repositories of the  
708 *Ag1000G* project Phase 2-AR1 (The *Anopheles gambiae* 1000 Genomes Consortium 2017). Accession  
codes are available in Supplementary Material SM1 and download instructions can be found in  
710 the above-mentioned GitHub repository.

## Acknowledgements

712 We thank Arjèn Van 't Hof and Eric Lucas (LSTM) for fruitful discussions on the manuscript and  
its methods. We also thank Chris Clarkson (Wellcome Sanger Institute) for making his code  
714 publicly available.

This work was supported by the National Institute of Allergy and Infectious Diseases (R01-  
716 AI116811); the Wellcome Trust (090770/Z/09/Z; 090532/Z/09/Z; 098051); the Medical Research  
Council UK and the Department for International Development (MR/M006212/1) and the Medical  
718 Research Council (MR/P02520X/1). The latter grant is a UK funded award and is part of the  
EDCTP2 programme supported by the European Union. The content of this manuscript is solely  
720 the responsibility of the authors and does not necessarily represent the official views of the  
National Institute of Allergy and Infectious Diseases, or the National Institutes of Health.

## 722 Author contributions

XGB, MD and DW designed the study. XGB carried out the analyses of sequence diversity, selection  
724 and introgression, with assistance and code contribution from ST, NJH and AM. AOR carried out  
the structural modelling analyses. The *Ag1000G* Consortium undertook collection, preparation,  
726 sequencing, and primary analysis of the samples. All authors read and approved the final  
manuscript.

## 728 Competing interests

The authors declare no competing interests.

## 730 **Supplementary legends**

**Supplementary Material SM1. Data sources.** List of genome samples from *Ag1000G* Phase 2-AR1 (table A), the Phase 1-AR3 subset (table B) (both of which contain *A. gambiae* and *A. coluzzii* specimens), and outgroup species (table C; includes *A. arabiensis*, *A. quadriannulatus*, *A. christyi*, *A. epiroticus*, *A. merus* and *A. melas*). For each sample, we include their country and population of origin, accession numbers (based on *Ag1000G* for Phase 1 and 2, and on NCBI SRA for outgroups), and the estimated 2La karyotypes.

**Supplementary Material SM2. List of genetic variants in *Rdl*.** **A)** List of all variants present in the *Rdl* gene (AGAP006028), including their genomic coordinates, reference and alternative alleles, coordinates of the mutation along *Rdl* CDS and peptide sequences, effect on the peptide sequence (aminoacid substitution), and frequencies in each of the populations of the cohort (Phase 2 and outgroups). **B)** Genotypes of *Rdl* non-synonymous mutations in each sample (for the six mutations reported in Figure 1), where 0=wt homozygote, 1=heterozygote, 2=alternate allele homozygote.

**Supplementary Material SM3. Linkage disequilibrium in *Rdl*.** Linkage disequilibrium between non-synonymous mutations in *Rdl*, separated by population. Only populations where non-synonymous variants are shown are displayed. For each population, we display Huff and Rogers'  $r$  (left) and Lewontin's  $D'$  (right).

**Supplementary Material SM4. Alignments of *Rdl* orthologs.** **A)** Alignment of *Rdl* orthologs from 12 species from the Culicidae family: *A. gambiae* (Anogam), *A. arabiensis* (Anoara), *A. atroparvus* (Anoatr), *A. darlingi* (Anodar), *A. dirus* (Anodir), *A. epiroticus* (Anoepi), *A. farauti* (Anofar), *A. funestus* (Anofun), *A. merus* (Anomer), *A. minimus* (Anomin), and *Aedes aegypti* (Aedaeg). Pfam-predicted protein domains, transmembrane regions and the 296 and 345 codons are shown on top of the alignment (coordinates based on the *A. gambiae* ortholog). **B-C)** Pairwise sequence identity and  $d_N/d_S$  between *Rdl* orthologs, including all *A. gambiae* isoforms (RA, RB, RC).

**Supplementary Material SM5. Haplotype classification and population frequency.** **A)** Clustering of haplotypes according to the minimum spanning networks (built from 626 phased variants located around codon 296; Figure 3 and Supplementary Material SM6). For each cluster, we report their population and country of origin, species, and allele present in *Rdl* codon 296 (*296G*, *296S*, *wt*) and *Vgsc* codon 995 (*995F*, *995S* and *wt*). Cluster "4" includes haplotypes with *296G* alleles, cluster "34" includes *296S* alleles; all other clusters are *wt*. **B)** Absolute frequency of *296G*, *296S* and *wt* haplotype clusters per population.

**Supplementary Material SM6. Minimum spanning networks of *Rdl* haplotypes.** Minimum spanning

networks of haplotypes around *Rdl* codon 296 (626 phased variants located +/- 10,000 bp from the 2L:25429236 position), including all non-singleton haplotype clusters. Purple arrows indicate the direction of non-synonymous mutations (relative to reference assembly). **A)** Nodes are color-coded according to genotype in *Rdl* codon 296. **B)** Nodes are color-coded according to genotype in *Vgsc* codon 995. **C)** Nodes are color-coded according to species.

**Supplementary Material SM7. Linkage disequilibrium of *Rdl* and *Vgsc*.** Linkage disequilibrium between non-synonymous mutations in *Rdl* and *Vgsc*, calculated using Huff and Rogers'  $r$  (A) and Lewontin's  $D'$  (B). Resistance variants in both genes are highlighted in orange (*Vgsc*) and cerise red (*Rdl*).

**Supplementary Material SM8. Co-segregation of *Rdl* and *Vgsc* mutations. A-B)** Frequency of alleles in *Vgsc* codon 995 and *Rdl* codon 296 per population, calculated per chromosome. Note: *A. gambiae* populations denoted with an asterisk (The Gambia, Guinea-Bissau and Kenya) are listed separately due to their high frequency of hybridisation and/or unclear species identification (see Methods). **C)** Geographical co-occurrence of *Rdl* and *Vgsc* mutations, at 10% and 30% frequency thresholds (chosen for illustrative purposes). Dots indicate presence. **D)** Euler diagrams and contingency table depicting the co-occurrence of *Vgsc* 995F and 995S alleles with *Rdl* 296G, 296S and *wt* alleles within chromosomes analysed in this study ( $n = 2356$ ). For chromosomes carrying each of the *Rdl* haplotype groups, we include the percentage of associated genotypes at *Vgsc* codon 995. **E)** Number of chromosomes carrying 296S or 296G mutations (x axis) against number of 995F mutations (y axis), per population (only values >0 included). **F)** Contingency tables of *Rdl* and *Vgsc* resistance mutations co-occurrence, per population. Only populations where resistance alleles in are segregating in both genes are included.  $p$  values and odds ratios [OR] correspond to Fisher's exact tests (one-sided, testing for a greater co-occurrence of *Rdl* codon 296 and *Vgsc* 995 resistance alleles).

**Supplementary Material SM9. PCA of 2La karyotypes.** Principal component (PC) analysis of allele presence/absence from 10,000 random variants located within the 2La inversion (coordinates: 2L:20524058-42165532). Specimens from *Ag1000G* Phase 1 and *A. arabiensis* are color-coded by 2La genotype (homozygotes and heterozygotes, blue-purple), and they are used as a reference to assign 2La genotypes to Phase 2 specimens (grey). Panels A and B show PC1, PC2 and PC3; panel C shows the fraction of variance explained by each PC. The 2La karyotypes of all Phase 2 specimens are available in Supplementary Material SM1.

**Supplementary Material SM10. Alignments of *Rdl* haplotypes. A)** 5' start of the gene (2L:25363652, 696 variants). **B)** 3' end of the gene (2L:25434556, 428 variants). **C)** Unadmixed upstream region within the 2La inversion (1 Mb upstream of *Rdl*; 2903 variants). **D)** Unadmixed downstream region



within the 2La inversion (1 Mb downstream of *Rdl*, 2594 variants). The name of each sequence name indicates the specimen (codes from Supplementary Material SM1; e.g. AA0040-C), haplotype (a or b), population of origin (e.g. GHcol), genotype at codon 296 (gt0=wt, gt1=296G, gt2=296S), and 2La background (kt0=2L<sup>+</sup>/2L<sup>+</sup>, kt1=2La/2L<sup>+</sup>, kt2=2La/2La).

**Supplementary Material SM11. Phylogenies of *Rdl* haplotypes.** Phylogenetic trees from alignments around the *Rdl* locus (Supplementary Material SM10), in Newick format and including ultrafast bootstrap (UFBS) statistical supports. The name of each sequence (e.g. “AA0040-Ca\_GHcol\_gt0\_kt0”) indicates the specimen (codes from Supplementary Material SM1; “AA0040-C”), chromosome (“a” or “b”), population of origin (“GHcol”), allele at codon 296 (gt0=wt, gt1=296G, gt2=296S), and 2La karyotype (kt0=2L<sup>+</sup>/2L<sup>+</sup>, kt1=2La/2L<sup>+</sup>, kt2=2La/2La).

**Supplementary Material SM12. 296S introgression between *A. coluzzii* and *A. arabiensis*.** **A)** Profile of Patterson’s *D* in 2La/2La backgrounds, using *A. coluzzii* specimens as populations A and B (296S and *wt*, respectively); *A. arabiensis* as population C (296S as positive controls, *wt* as test), *A. merus* as a negative control for population C (*wt*); and either *A. christyi* or *A. epiroticus* as outgroups (*wt*). **B)** Profile of Patterson’s *D* in 2La/2La backgrounds, using *A. arabiensis* specimens as populations A and B (296G and *wt*, respectively); *A. coluzzii* as population C (296S as positive controls, *wt* as test), *A. merus* as a negative control for population C (*wt*); and either *A. christyi* or *A. epiroticus* as outgroups (*wt*).

In all panels, the hypothesis under test can be summarised as follows: if 296S homozygotes from species *i* show evidence of introgression with *wt* homozygotes from species *j* but not with *wt* from *i*, it means that 296S originated in species *j*. Left plots depict the entire 2L chromosomal arm (orange lines demarcate 2La inversion), and rightmost plots focus on the *Rdl* locus (*Rdl* gene coordinates highlighted in red). *D* was calculated in sliding blocks of 10,000 phased variants (with 20% overlap). For each comparison, we report the mean value of *D* in the *Rdl* locus and use a block-jackknife procedure (block length = 100 variants) to estimate its standard error, a Z-score (standardized *D*) and *p*-value (that reflects deviation from the null expectation of *D* = 0).

**Supplementary Material SM13. 296G introgression between *A. gambiae* and *A. coluzzii*.** **A)** Profile of Patterson’s *D* in 2L<sup>+</sup>/2L<sup>+</sup> backgrounds, using *A. coluzzii* specimens as populations A and B (296G and *wt*, respectively); *A. gambiae* as population C (296G as positive controls, *wt* as test); and either *A. quadriannulatus* or *A. melas* as outgroups (*wt*). **B)** Profile of Patterson’s *D* in 2L<sup>+</sup> backgrounds, using *A. gambiae* specimens as populations A and B (296G and *wt*, respectively); *A. coluzzii* as population C (296G as positive control, *wt* as test); and either *A. quadriannulatus* or *A. melas* as outgroups (*wt*). **C)** Profile of Patterson’s *D* in 2La/2La backgrounds, using *A. coluzzii* specimens as populations A and B (296G and *wt*, respectively); *A. gambiae* as population C (296G as positive controls, *wt* as test); and *A. merus* as outgroup

(*wt*). **D**) Profile of Patterson's  $D$  in 2La/2La backgrounds, using *A. gambiae* specimens as populations A and B (296G and *wt*, respectively); *A. coluzzii* as population C (296G as positive controls, *wt* as test); and *A. merus* as outgroup (*wt*).

In all panels, the hypothesis under test can be summarised as follows: if 296G homozygotes from species  $i$  show evidence of introgression with *wt* homozygotes from species  $j$  but not with *wt* from  $i$ , it means that 296G originated in species  $j$ . Left plots depict the entire 2L chromosomal arm (orange lines demarcate 2La inversion), and rightmost plots focus on the *Rdl* locus (*Rdl* gene coordinates highlighted in red).  $D$  was calculated in sliding blocks of 10,000 phased variants (with 20% overlap). For each comparison, we report the mean value of  $D$  in the *Rdl* locus and use a block-jackknife procedure (block length = 100 variants) to estimate its standard error, a Z-score (standardized  $D$ ) and  $p$ -value (that reflects deviation from the null expectation of  $D = 0$ ).

**Supplementary Material SM14. Diversity of 296G haplotypes in 2L<sup>+</sup> and 2La backgrounds. A)**

Profile of  $EHH$  decay for each group of 296G haplotypes (296G in 2L<sup>+</sup>/2L<sup>+</sup>, 2La/2L<sup>+</sup> and 2La/2La backgrounds), built from 16,623 phased variants located  $\pm 150,000$  bp from codon 296 (2L:25429236 position). **B**) Profile of haplotypic diversity along chromosomal arm 2L (sliding blocks of 500 variants with 20% overlap). **C**) Absolute sequence divergence ( $D_{xy}$ ) between 296G alleles of 2L<sup>+</sup> background and *wt* resistance haplotypes of 2L<sup>+</sup> and 2La backgrounds. **D**) Absolute sequence divergence ( $D_{xy}$ ) between 296G alleles of 2La background and *wt* resistance haplotypes of 2L<sup>+</sup> and 2La backgrounds. All values are calculated in windows of 20,000 kbp with 10% overlap.

**Supplementary Material SM15. Genetic differentiation in the 2La inversion.** Differentiation

(Hudson's  $F_{ST}$ ) along the 2L chromosomal arm between *A. gambiae* and *A. coluzzii* species, separated by their 2La karyotype (2La/2La or 2L<sup>+</sup>/2L<sup>+</sup>). Panel A shows comparisons with *A. gambiae* with 2L<sup>+</sup>/2L<sup>+</sup> karyotypes, and panel B for *A. gambiae* with 2La/2La karyotypes.  $F_{ST}$  estimates have been calculated in adjacent blocks of 5,000 phased variants with 20% overlap. Sub-panels at the right focus on the *Rdl* genomic locus. Note that interkaryotype comparisons have higher  $F_{ST}$  in the 2La region than inter-species comparisons.

## References

- 732 Andolfatto P, Depaulis F, Navarro A. 2001. Inversion polymorphisms and nucleotide variability in *Drosophila*. *Genet. Res.* 77:1–8.
- 734 Asahi M, Kobayashi M, Matsui H, Nakahira K. 2015. Differential mechanisms of action of the novel  $\gamma$ -aminobutyric acid receptor antagonist ectoparasiticides fluralaner (A1443) and fipronil. *Pest Manag. Sci.* 71:91–95.
- 736 Van der Auwera GA, Carneiro MO, Hartl C, Poplin R, del Angel G, Levy-Moonshine A, Jordan T, Shakir K, Roazen D, Thibault J, et al. 2013. From fastQ data to high-confidence variant calls: The genome analysis toolkit best practices pipeline. *Curr. Protoc. Bioinforma.* 11:11.10.1.
- 738 Ayala D, Zhang S, Chateau M, Fouet C, Morlais I, Costantini C, Hahn MW, Besansky NJ. 2019. Association mapping desiccation resistance within chromosomal inversions in the African malaria vector *Anopheles gambiae*. *Mol. Ecol.* 28:1333–1342.
- 740 Ayala FJ, Coluzzi M. 2005. Chromosome speciation: humans, *Drosophila*, and mosquitoes. *Proc. Natl. Acad. Sci.* 102 Suppl:6535–6542.
- 742 Bandelt HJ, Forster P, Rohl A. 1999. Median-joining networks for inferring intraspecific phylogenies. *Mol. Biol. Evol.* 16:37–48.
- 746 van den Berg H, Zaim M, Yadav RS, Soares A, Ameneshewa B, Mnzava A, Hii J, Dash AP, Ejov M. 2012. Global Trends in the Use of Insecticides to Control Vector-Borne Diseases. *Environ. Health Perspect.* 120:577–582.
- 748 Chaccour CJ, Kobylinski KC, Bassat Q, Bousema T, Drakeley C, Alonso P, Foy BD. 2013. Ivermectin to reduce malaria transmission: A research agenda for a promising new tool for elimination. *Malar. J.* 12:153.
- 750 Charif D, Lobry JR. 2007. SeqinR 1.0-2: a contributed package to the R project for statistical computing devoted to biological sequences retrieval and analysis. In: Bastolla U, Porto M, Roman HE, Vendruscolo M, editors. *Structural approaches to sequence evolution: Molecules, networks, populations. Biological and Medical Physics, Biomedical Engineering.* New York: Springer Verlag. p. 207–232.
- 752 ChemAxon. 2019. ChemAxon. Available from: <https://chemaxon.com/>
- 754 Cheng C, White BJ, Kamdem C, Mockaitis K, Costantini C, Hahn MW, Besansky NJ. 2012. Ecological Genomics of *Anopheles gambiae* Along a Latitudinal Cline: A Population-Resequencing Approach. *Genetics* 190:1417–1432.
- 756 Chovnick A. 1973. Gene conversion and transfer of genetic information within the inverted region of inversion heterozygotes. *Genetics* 75:123–131.
- 758 Cingolani P, Platts A, Wang LL, Coon M, Nguyen T, Wang L, Land SJ, Lu X, Ruden DM. 2012. A program for annotating and predicting the effects of single nucleotide polymorphisms, SnpEff: SNPs in the genome of *Drosophila melanogaster* strain w1118; iso-2; iso-3. *Fly (Austin)*. 6:80–92.
- 760 Clarkson CS, Miles A, Harding NJ, Weetman D, Kwiatkowski D, Donnelly M, The *Anopheles gambiae* 1000 Genomes Consortium. 2018. The genetic architecture of target-site resistance to pyrethroid insecticides in the African malaria vectors *Anopheles gambiae* and *Anopheles coluzzii*. *BioRxiv*.
- 764 Clarkson CS, Weetman D, Essandoh J, Yawson AE, Maslen G, Manske M, Field SG, Webster M, Antão T, MacInnis B, et al. 2014. Adaptive introgression between *Anopheles* sibling species eliminates a major genomic island but not reproductive isolation. *Nat. Commun.* 5:4248.
- 766 Coluzzi M. 2002. A Polytene Chromosome Analysis of the *Anopheles gambiae* Species Complex. *Science (80-.)*. 298:1415–1418.
- 770

- Coluzzi M, Sabatini A, Petrarca V, Di Deco MA. 1979. Chromosomal differentiation and adaptation to human  
772 environments in the *Anopheles gambiae* complex. *Trans. R. Soc. Trop. Med. Hyg.* 73:483–497.
- Davidson G. 1956. Insecticide resistance in *Anopheles gambiae* Giles: a case of simple mendelian inheritance.  
774 *Nature* 178:863–864.
- Davidson G, Hamon J. 1962. A Case of Dominant Dieldrin Resistance in *Anopheles gambiae* Giles. *Nature*  
776 196:1012–1012.
- Davies TGE, Field LM, Usherwood PNR, Williamson MS. 2007. A comparative study of voltage-gated sodium  
778 channels in the Insecta: implications for pyrethroid resistance in Anopheline and other Neopteran species.  
*Insect Mol. Biol.* 16:361–375.
- 780 Delaneau O, Howie B, Cox AJ, Zagury JF, Marchini J. 2013. Haplotype estimation using sequencing reads. *Am. J.*  
*Hum. Genet.* 93:687–696.
- 782 Du W, Awolola TS, Howell P, Koekemoer LL, Brooke BD, Benedict MQ, Coetzee M, Zheng L. 2005. Independent  
mutations in the *Rdl* locus confer dieldrin resistance to *Anopheles gambiae* and *An. arabiensis*. *Insect Mol.*  
784 *Biol.* 14:179–183.
- Durand EY, Patterson N, Reich D, Slatkin M. 2011. Testing for Ancient Admixture between Closely Related  
786 Populations. *Mol. Biol. Evol.* 28:2239–2252.
- Elliott R, Ramakrishna V. 1956. Insecticide resistance in *Anopheles gambiae* Giles. *Nature* 177:532–533.
- 788 Ellson J, Gansner E, Hu Y, Janssen E, North S. Graphviz - Graph Visualization Software. Available from:  
<https://www.graphviz.org/about/>
- 790 Eswar N, Webb B, Marti-Renom MA, Madhusudhan MS, Eramian D, Shen M-Y, Pieper U, Sali A. 2006. Comparative  
Protein Structure Modeling Using Modeller. *Curr. Protoc. Bioinforma.* 15:5.6.1-5.6.30.
- 792 ffrench-Constant RH, Anthony N, Aronstein K, Rocheleau T, Stilwell G. 2000. Cyclodiene Insecticide Resistance:  
From Molecular to Population Genetics. *Annu. Rev. Entomol.* 45:449–466.
- 794 ffrench-Constant RH, Bass C. 2017. Does resistance really carry a fitness cost? *Curr. Opin. Insect Sci.* 21:39–46.
- ffrench-Constant RH, Rocheleau TA, Steichen JC, Chalmers AE. 1993. A point mutation in a *Drosophila* GABA  
796 receptor confers insecticide resistance. *Nature* 363:449–451.
- ffrench-Constant RH, Steichen JC, Rocheleau TA, Aronstein K, Roush RT. 1993. A single-amino acid substitution in  
798 a gamma-aminobutyric acid subtype A receptor locus is associated with cyclodiene insecticide resistance in  
*Drosophila* populations. *Proc. Natl. Acad. Sci. U. S. A.* 90:1957–1961.
- 800 Fontaine MC, Pease JB, Steele A, Waterhouse RM, Neafsey DE, Sharakhov I V., Jiang X, Hall AB, Catteruccia F,  
Kakani E, et al. 2015. Extensive introgression in a malaria vector species complex revealed by  
802 phylogenomics. *Science* (80-.). 347:1258524.
- Gant DB, Chalmers AE, Wolff MA, Hoffman HB, Bushey D. 1998. Fipronil: action at the GABA receptor. In: Kuhr RJ,  
804 Motoyama N, editors. *Pesticides and the Future*. IOS Press. p. 147–156.
- Garud NR, Messer PW, Buzbas EO, Petrov DA. 2015. Recent Selective Sweeps in North American *Drosophila*  
806 *melanogaster* Show Signatures of Soft Sweeps. Copenhaver GP, editor. *PLOS Genet.* 11:e1005004.
- Gielen M, Thomas P, Smart TG. 2015. The desensitization gate of inhibitory Cys-loop receptors. *Nat. Commun.*  
808 6:6829.
- Giraldo-Calderón GI, Emrich SJ, MacCallum RM, Maslen G, Dialynas E, Topalis P, Ho N, Gesing S, Madey G, Collins  
810 FH, et al. 2015. VectorBase: an updated bioinformatics resource for invertebrate vectors and other  
organisms related with human diseases. *Nucleic Acids Res.* 43:D707–D713.

- 812 Le Goff G, Hamon A, Bergé JJ-B, Amichot M, Goff G Le, Hamon A, Bergé JJ-B, Amichot M. 2005. Resistance to  
fipronil in *Drosophila simulans*: influence of two point mutations in the RDL GABA receptor subunit. *J.*  
814 *Neurochem.* 92:1295–1305.
- Guex N, Diemand A, Peitsch MC. 1999. Protein modelling for all. *Trends Biochem. Sci.* 24:364–367.
- 816 Hoang DT, Chernomor O, von Haeseler A, Minh BQ, Vinh LS. 2018. UFBoot2: Improving the Ultrafast Bootstrap  
Approximation. *Mol. Biol. Evol.* 35:518–522.
- 818 Hoerauf A, Pfarr K, Mand S, Debrah AY, Specht S. 2011. Filariasis in Africa-treatment challenges and prospects.  
*Clin. Microbiol. Infect.* 17:977–985.
- 820 Katoh K, Standley DM. 2013. MAFFT multiple sequence alignment software version 7: improvements in  
performance and usability. *Mol. Biol. Evol.* 30:772–780.
- 822 Kirkpatrick M. 2010. How and Why Chromosome Inversions Evolve. *PLoS Biol.* 8:e1000501.
- Kolde R. 2019. pheatmap: Pretty Heatmaps.
- 824 Kwiatkowska RM, Platt N, Poupardin R, Irving H, Dabire RK, Mitchell S, Jones CM, Diabaté A, Ranson H, Wondji CS.  
2013. Dissecting the mechanisms responsible for the multiple insecticide resistance phenotype in  
826 *Anopheles gambiae* s.s., M form, from Vallée du Kou, Burkina Faso. *Gene* 519:98–106.
- Lawniczak MKN, Emrich SJ, Holloway AK, Regier AP, Olson M, White B, Redmond S, Fulton L, Appelbaum E,  
828 Godfrey J, et al. 2010. Widespread Divergence Between Incipient *Anopheles gambiae* Species Revealed by  
Whole Genome Sequences. *Science* (80-. ). 330:512–514.
- 830 Lewontin RC. 1964. The Interaction of Selection and Linkage. I. General Considerations; Heterotic Models.  
*Genetics* 49:49–67.
- 832 Li H, Durbin R. 2009. Fast and accurate short read alignment with Burrows-Wheeler transform. *Bioinformatics*  
25:1754–1760.
- 834 Lucas ER, Miles A, Harding NJ, Clarkson CS, Lawniczak MKN, Kwiatkowski DP, Weetman D, Donnelly MJ. 2019.  
Whole-genome sequencing reveals high complexity of copy number variation at insecticide resistance loci  
836 in malaria mosquitoes. *Genome Res.* 29:1250–1261.
- Lynd A, Weetman D, Barbosa S, Egyir Yawson A, Mitchell S, Pinto J, Hastings I, Donnelly MJ. 2010. Field, Genetic,  
838 and Modeling Approaches Show Strong Positive Selection Acting upon an Insecticide Resistance Mutation in  
*Anopheles gambiae* s.s. *Mol. Biol. Evol.* 27:1117–1125.
- 840 Macoris M de L, Martins AJ, Andrighetti MTM, Lima JBP, Valle D. 2018. Pyrethroid resistance persists after ten  
years without usage against *Aedes aegypti* in governmental campaigns: Lessons from São Paulo State,  
842 Brazil. Kittayapong P, editor. *PLoS Negl. Trop. Dis.* 12:e0006390.
- Martinez-Torres D, Chandre F, Williamson MS, Darriet F, Berge JB, Devonshire AL, Guillet P, Pasteur N, Pauron D.  
844 1998. Molecular characterization of pyrethroid knockdown resistance (kdr) in the major malaria vector  
*Anopheles gambiae* s.s. *Insect Mol. Biol.* 7:179–184.
- 846 Masiulis S, Desai R, Uchański T, Serna Martin I, Laverty D, Karia D, Malinauskas T, Zivanov J, Pardon E, Kotecha A,  
et al. 2019. GABAA receptor signalling mechanisms revealed by structural pharmacology. *Nature* 565:454–  
848 459.
- Messer PW, Petrov DA. 2013. Population genomics of rapid adaptation by soft selective sweeps. *Trends Ecol. Evol.*  
850 28:659–669.
- Miglianico M, Eldering M, Slater H, Ferguson N, Ambrose P, Lees RS, Koolen KMJ, Pruzinova K, Jancarova M, Volf P,  
852 et al. 2018. Repurposing isoxazoline veterinary drugs for control of vector-borne human diseases. *Proc.*

Natl. Acad. Sci. U. S. A. 115:E6920–E6926.

- 854 Miles A, Harding N. 2017. scikit-allel. Available from: <https://github.com/cggh/scikit-allel>
- Miles A, Harding NJ, Bottà G, Clarkson CS, Antão T, Kozak K, Schrider DR, Kern AD, Redmond S, Sharakhov I, et al.  
856 2017. Genetic diversity of the African malaria vector *Anopheles gambiae*. *Nature* 552:96–100.
- Minh BQ, Nguyen MAT, von Haeseler A. 2013. Ultrafast approximation for phylogenetic bootstrap. *Mol. Biol. Evol.*  
858 30:1188–1195.
- Morris GM, Huey R, Lindstrom W, Sanner MF, Belew RK, Goodsell DS, Olson AJ. 2009. AutoDock4 and  
860 AutoDockTools4: Automated docking with selective receptor flexibility. *J. Comput. Chem.* 30:2785–2791.
- Nakao T, Banba S. 2015. Minireview: Mode of action of meta-diamide insecticides. *Pestic. Biochem. Physiol.*  
862 121:39–46.
- Nakao T, Banba S, Hirase K. 2015. Comparison between the modes of action of novel meta-diamide and  
864 macrocyclic lactone insecticides on the RDL GABA receptor. *Pestic. Biochem. Physiol.* 120:101–108.
- Nakao T, Banba S, Nomura M, Hirase K. 2013. Meta-diamide insecticides acting on distinct sites of RDL GABA  
866 receptor from those for conventional noncompetitive antagonists. *Insect Biochem. Mol. Biol.* 43:366–375.
- Neafsey DE, Waterhouse RM, Abai MR, Aganezov SS, Alekseyev MA, Allen JE, Amon J, Arcà B, Arensburger P,  
868 Artemov G, et al. 2015. Highly evolvable malaria vectors: The genomes of 16 *Anopheles* mosquitoes. *Science*  
(80- ). 347:1258522.
- 870 Nguyen L-TT, Schmidt HA, Von Haeseler A, Minh BQ. 2015. IQ-TREE: a fast and effective stochastic algorithm for  
estimating maximum-likelihood phylogenies. *Mol. Biol. Evol.* 32:268–274.
- 872 Oxborough RM. 2016. Trends in US President’s Malaria Initiative-funded indoor residual spray coverage and  
insecticide choice in sub-Saharan Africa (2008–2015): urgent need for affordable, long-lasting insecticides.  
874 *Malar. J.* 15:146.
- Ozoe Y, Asahi M, Ozoe F, Nakahira K, Mita T. 2010. The antiparasitic isoxazoline A1443 is a potent blocker of  
876 insect ligand-gated chloride channels. *Biochem. Biophys. Res. Commun.* 391:744–749.
- Page AJ, Taylor B, Delaney AJ, Soares J, Seemann T, Keane JA, Harris SR. 2016. SNP-sites: rapid efficient  
878 extraction of SNPs from multi-FASTA alignments. *Microb. Genomics* 2.
- Paradis E, Claude J, Strimmer K. 2004. APE: Analyses of Phylogenetics and Evolution in R language.  
880 *Bioinformatics* 20:289–290.
- Paradis E, Schliep K. 2019. ape 5.0: an environment for modern phylogenetics and evolutionary analyses in  
882 R. Schwartz R, editor. *Bioinformatics* 35:526–528.
- Patterson N, Moorjani P, Luo Y, Mallick S, Rohland N, Zhan Y, Genschoreck T, Webster T, Reich D. 2012. Ancient  
884 Admixture in Human History. *Genetics* 192:1065–1093.
- Pedregosa F, Varoquaux G, Gramfort A, Michel V, Thirion B, Grisel O, Blondel M, Prettenhofer P, Weiss R, Dubourg  
886 V, et al. 2011. Scikit-learn: Machine Learning in Python. *J. Mach. Learn. Res.* 12:2825–2830.
- Platt N, Kwiatkowska RM, Irving H, Diabaté A, Dabire R, Wondji CS. 2015. Target-site resistance mutations (kdr  
888 and RDL), but not metabolic resistance, negatively impact male mating competitiveness in the malaria vector  
*Anopheles gambiae*. *Heredity (Edinb)*. 115:243–252.
- 890 R Core Team. 2017. R: A Language and Environment for Statistical Computing.
- Ranson H, N’Guessan R, Lines J, Moiroux N, Nkuni Z, Corbel V. 2011. Pyrethroid resistance in African anopheline  
892 mosquitoes: what are the implications for malaria control? *Trends Parasitol.* 27:91–98.

- 894 Remnant EJ, Morton CJ, Daborn PJ, Lumb C, Yang YT, Ng HL, Parker MW, Batterham P. 2014. The role of Rdl in  
resistance to phenylpyrazoles in *Drosophila melanogaster*. *Insect Biochem. Mol. Biol.* 54:11–21.
- 896 Revell LJ. 2012. phytools: an R package for phylogenetic comparative biology (and other things). *Methods Ecol.  
Evol.* 3:217–223.
- 898 Riehle MM, Bukhari T, Gneme A, Guelbeogo WM, Coulibaly B, Fofana A, Pain A, Bischoff E, Renaud F, Beavogui AH,  
et al. 2017. The *Anopheles gambiae* 2La chromosome inversion is associated with susceptibility to  
*Plasmodium falciparum* in Africa. *Elife* 6.
- 900 Rogers AR, Huff C. 2009. Linkage disequilibrium between loci with unknown phase. *Genetics* 182:839–844.
- 902 Rottschaefel SM, Riehle MM, Coulibaly B, Sacko M, Niaré O, Morlais I, Traoré SF, Vernick KD, Lazzaro BP. 2011.  
Exceptional Diversity, Maintenance of Polymorphism, and Recent Directional Selection on the APL1 Malaria  
Resistance Genes of *Anopheles gambiae*. Schneider DS, editor. *PLoS Biol.* 9:e1000600.
- 904 Rowland M. 1991a. Activity and mating competitiveness of gamma HCH/dieldrin resistant and susceptible male  
and virgin female *Anopheles gambiae* and *An. stephensi* mosquitoes, with assessment of an insecticide-rotation  
906 strategy. *Med. Vet. Entomol.* 5:207–222.
- 908 Rowland M. 1991b. Behaviour and fitness of gamma HCH/dieldrin resistant and susceptible female *Anopheles  
gambiae* and *An. stephensi* mosquitoes in the absence of insecticide. *Med. Vet. Entomol.* 5:193–206.
- 910 Rozas J, Aguadé M. 1994. Gene conversion is involved in the transfer of genetic information between naturally  
occurring inversions of *Drosophila*. *Proc. Natl. Acad. Sci. U. S. A.* 91:11517–11521.
- Schrödinger L. 2015. The PyMOL Molecular Graphics System, Version 1.8.
- 912 Sievers F, Wilm A, Dineen D, Gibson TJ, Karplus K, Li W, Lopez R, McWilliam H, Remmert M, Söding J, et al. 2011.  
Fast, scalable generation of high-quality protein multiple sequence alignments using Clustal Omega. *Mol.  
914 Syst. Biol.* 7:539.
- 916 Smart OS, Neduvilil JG, Wang X, Wallace BA, Sansom MSP. 1996. HOLE: A program for the analysis of the pore  
dimensions of ion channel structural models. *J. Mol. Graph.* 14:354–360.
- 918 Stump AD, Pombi M, Goeddel L, Ribeiro JMC, Wilder JA, Torre AD, Besansky NJ. 2007. Genetic exchange in 2La  
inversion heterokaryotypes of *Anopheles gambiae*. *Insect Mol. Biol.* 16:703–709.
- 920 Sturtevant AH. 1917. Genetic Factors Affecting the Strength of Linkage in *Drosophila*. *Proc. Natl. Acad. Sci.* 3:555–  
558.
- 922 Suyama M, Torrents D, Bork P. 2006. PAL2NAL: robust conversion of protein sequence alignments into the  
corresponding codon alignments. *Nucleic Acids Res.* 34:W609–W612.
- 924 Takahata N, Nei M. 1985. Gene genealogy and variance of interpopulational nucleotide differences. *Genetics*  
110:325–344.
- 926 Taylor-Wells J, Brooke BD, Bermudez I, Jones AK. 2015. The neonicotinoid imidacloprid, and the pyrethroid  
deltamethrin, are antagonists of the insect Rdl GABA receptor. *J. Neurochem.* 135:705–713.
- 928 The *Anopheles gambiae* 1000 Genomes Consortium. 2017. Ag1000G Phase 2 AR1 data release. MalariaGEN  
[Internet]. Available from: <https://www.malariagen.net/data/ag1000g-phase-2-ar1>
- 930 The *Anopheles gambiae* 1000 Genomes Consortium. 2019. Genome variation and population structure among  
1,142 mosquitoes of the African malaria vector species *Anopheles gambiae* and *Anopheles coluzzii*.  
bioRxiv:864314.
- 932 Thompson M, Steichen JC, French-Constant RH. 1993. Conservation of cyclodiene insecticide resistance-  
associated mutations in insects. *Insect Mol. Biol.* 2:149–154.

- 934 Trott O, Olson AJ. 2009. AutoDock Vina: Improving the speed and accuracy of docking with a new scoring function, efficient optimization, and multithreading. *J. Comput. Chem.* 31:455–461.
- 936 Tukey J. 1958. Bias and Confidence in Not-quite Large Samples. *Ann. Math. Stat.* 29:614–623.
- Vicente JL, Clarkson CS, Caputo B, Gomes B, Pombi M, Sousa CA, Antao T, Dinis J, Bottà G, Mancini E, et al. 2017.
- 938 Massive introgression drives species radiation at the range limit of *Anopheles gambiae*. *Sci. Rep.* 7:46451.
- Weetman D, Wilding CS, Neafsey DE, Müller P, Ochomo E, Isaacs AT, Steen K, Rippon EJ, Morgan JC, Mawejje HD, et al. 2018. Candidate-gene based GWAS identifies reproducible DNA markers for metabolic pyrethroid resistance from standing genetic variation in East African *Anopheles gambiae*. *Sci. Rep.* 8:2920.
- 940
- 942 Wickham H. 2019. stringr: Simple, Consistent Wrappers for Common String Operations.
- Wondji CS, Dabire RK, Tukur Z, Irving H, Djouaka R, Morgan JC. 2011. Identification and distribution of a GABA receptor mutation conferring dieldrin resistance in the malaria vector *Anopheles funestus* in Africa. *Insect Biochem. Mol. Biol.* 41:484–491.
- 944
- 946 World Health Organization. 2012. Global plan for insecticide resistance management in malaria vectors. Genève: World Health Organization
- 948 Yang C, Huang Z, Li M, Feng X, Qiu X. 2017. RDL mutations predict multiple insecticide resistance in *Anopheles sinensis* in Guangxi, China. *Malar. J.* 16:482.